Water Resources Research

RESEARCH ARTICLE
10.1029/2019WR026449

High Resolution Modeling of River-Floodplain-Reservoir Inundation Dynamics in the Mekong River Basin

Sanghoon Shin[1], Yadu Pokhrel[1], Dai Yamazaki[2], Xiaodong Huang[3], Nathan Torbick[3], Jiaguo Qi[4], Sura Pattanakiat[5], Thanh Ngo-Duc[6], and Tuan Duc Nguyen[7]

[1]Department of Civil and Environmental Engineering, Michigan State University, East Lansing, MI, USA, [2]Institute of Industrial Science, The University of Tokyo, Komaba, Tokyo, Japan, [3]Applied Geosolutions, Durham, NH, USA, [4]Center for Global Change and Earth Observations, Michigan State University, East Lansing, MI, USA, [5]Faculty of Environment and Resource Studies, Mahidol University, Nakhonpathom, Thailand, [6]Department of Space and Aeronautics, University of Science and Technology of Hanoi, Vietnam Academy of Science and Technology, Hanoi, Vietnam, [7]Mekong River Commission, Vientiane, Lao PDR

Abstract Numerous studies have examined the changes in streamflow in the Mekong River Basin (MRB) using observations and hydrological modeling; however, there is a lack of integrated modeling studies that explicitly simulate the natural and human-induced changes in flood dynamics over the entire basin. Here we simulate the river-floodplain-reservoir inundation dynamics over the MRB for 1979–2016 period using a newly integrated, high-resolution (~5 km) river hydrodynamics-reservoir operation model. The framework is based on the river-floodplain hydrodynamic model CaMa-Flood in which a new reservoir operation scheme is incorporated by including 86 existing MRB dams. The simulated flood extent is downscaled to a higher resolution (~90 m) to investigate fine-scale inundation dynamics, and results are validated with ground- and satellite-based observations. It is found that the historical variations in surface water storage have been governed primarily by climate variability; the impacts of dams on river-floodplain hydrodynamics were marginal until 2009. However, results indicate that the dam impacts increased noticeably in 2010 when the basin-wide storage capacity doubled due to the construction of new mega dams. Further, results suggest that the future flood dynamics in the MRB would be considerably different than in the past even without climate change and additional dams. However, it is also found that the impacts of dams can largely vary depending on reservoir operation strategies. This study is expected to provide the basis for high-resolution river-floodplain-reservoir modeling for a holistic assessment of the impacts of dams and climate change on the floodpulse-dependent hydro-ecological systems in the MRB and other global regions.

Key Points:
- A high-resolution model is presented for the integrated simulation of river-floodplain-reservoir inundation dynamics
- Historical impacts of dams on the Mekong River flood dynamics are found to be marginal compared to that of climate variability
- Potential future dam impacts on the Mekong flood dynamics could be largely different than today even under business-as-usual conditions

Supporting Information:
- Supporting Information S1

Correspondence to:
Y. Pokhrel,
ypokhrel@egr.msu.edu

Citation:
Shin, S., Pokhrel, Y., Yamazaki, D., Huang, X., Torbick, N., Qi, J., et al. (2020). High resolution modeling of river-floodplain-reservoir inundation dynamics in the Mekong River Basin. *Water Resources Research*, *56*, e2019WR026449. https://doi.org/10.1029/2019WR026449

Received 30 SEP 2019
Accepted 22 MAR 2020
Accepted article online 14 APR 2020

1. Introduction

The construction of large dams accelerated globally during the latter half of the twentieth century, increasing global reservoir impoundment to a reported capacity of 7,000–10,000 km^3 (Chao et al., 2008; Lehner et al., 2011; Pokhrel, Hanasaki, Yeh, et al., 2012), which is equivalent to 16–25% of annual continental river discharge to the global oceans (Lehner et al., 2011; Oki & Kanae, 2006). Such large impoundment and flow regulation by dams are known to have dramatically altered natural flow regimes and fragmented most of the large global river systems (Dynesius & Nilsson, 1994; Graf, 1999; Nilsson et al., 2005). As river systems get fragmented, natural inundation dynamics is interrupted (Angarita et al., 2018; Mateo et al., 2014; Shin et al., 2019), fish migration pathways are often blocked, and downstream sediment delivery is impeded (Gupta et al., 2012; Renwick et al., 2005; Stone, 2016; Ziv et al., 2012), which can collectively cause profound hydrological, geomorphological, socio-ecological, and environmental changes in the downstream riverine and delta regions (Bunn & Arthington, 2002; Fencl et al., 2015; Poff & Schmidt, 2016; Tan et al., 2005; Vörösmarty et al., 2010; P. Wang et al., 2014; Wei et al., 2009; World Commission on Dams, 2000). Importantly, the adverse impact of alterations in river flow and flood dynamics can be potentially disruptive (Pokhrel, Shin et al., 2018) and "characteristically irreversible" (Latrubesse et al., 2017). Due to such adverse effects, dam removal is on the rise in regions with aging dams such as the United States (Null et al., 2014; Pohl, 2002); concomitantly, there is an unprecedented boom in dam construction in the developing world to satisfy growing energy needs (Timpe & Kaplan, 2017; Zarfl et al., 2015). The Mekong River Basin

(MRB) is one such region experiencing rapid expansion in large-scale hydropower dam construction (Grumbine & Xu, 2011; Pokhrel, Burbano, et al., 2018; Winemiller et al., 2016).

The Mekong is a transboundary river (Figure 1) shared by six countries (i.e., China, Myanmar, Thailand, Laos, Cambodia, and Vietnam). The river extends from the Tibetan Plateau (5,200 m altitude) to the South China Sea with 4,800 km of mainstem length and 795,000 km^2 of drainage area (Pokhrel, Shin, et al., 2018). Due to the snowmelt-based runoff in the Upper MRB (UMRB) at high elevation, and heavy monsoonal rainfall in the lower portion of the basin, the Mekong flow is characterized by a strong and pronounced unimodal flow pattern, known as the flood pulse (Junk et al., 1989). Wetlands and deepwater habitats as well as fisheries and agriculture systems that form the basis of local people's livelihoods have evolved with the natural rhythm of the seasonal flood pulse (Arias et al., 2019; Fredén, 2011). A distinct hydrological feature of the MRB is the flow reversal of the Tonle Sap River (TSR; Figure 1), which links the mainstem Mekong and Tonle Sap Lake (TSL; Figure 1) that serves as a natural detention reservoir. The TSL stores a large volume of water during the flooding period (June–October), supplied primarily (>50%; Pokhrel, Shin et al., 2018) by the reversed flow in the TSR, reaching a maximum of ~10,000 m^3/s (MRC, 2005); the water is discharged back to the Mekong River during the dry period (October–June).

The MRB is less dammed than other large global river basins (Grumbine & Xu, 2011); however, as dam construction continues (Pokhrel, Burbano, et al., 2018), it is feared that the hydro-ecological functioning of the river could be permanently altered, potentially to an irreversible level (Burbano et al., 2020; Pokhrel, Shin, et al., 2018; Sabo et al., 2017; Stone, 2016; Ziv et al., 2012). Further, climate-induced changes in temperature and rainfall patterns (Delgado et al., 2012) and sea level rise (Erban et al., 2014; Smajgl et al., 2015) add further stress to the continually evolving river flow and flood dynamics. Floodplain is a habitat used by many species for spawning, feeding, nursing, and refuge (Grill et al., 2019; Jardine et al., 2012), and the spatiotemporal dynamics of inundation is known to play a key role in the functioning of floodplain ecosystems (Górski et al., 2012; Jardine et al., 2012; Warfe et al., 2013). Hence, it has become increasingly imperative to better understand the changing inundation dynamics of the MRB and thereby predict its future evolution under projected water resource development (especially dam construction) and climate change.

The understanding of inundation dynamics in the entire MRB is currently limited. Observation-based studies have reported a shift in flow patterns after the construction of dams (e.g., Räsänen et al., 2012; Sabo et al., 2017; W. Wang et al., 2017); however, these studies have not examined the dynamics of inundation extent, due to data limitations. There has been an increase in model-based studies in the past decade; however, those studies have focused on some parts of the MRB such as the UMRB (e.g., Dang et al., 2019; Han et al., 2019; Räsänen et al., 2012), Lower MRB (LMRB) (e.g., Dang et al., 2018; Trung et al., 2018), the 3S-river system (e.g., Wild & Loucks, 2014), Mun river basin (e.g., Akter & Babel, 2012), and TSL and the Mekong Delta regions (e.g., Arias, Piman, et al., 2014; Duc Tran et al., 2018; Minh et al., 2019; Oeurng et al., 2019; Smajgl et al., 2015). There are some basin-wide modeling studies (e.g., Lauri et al., 2012; Piman et al., 2013; Sridhar et al., 2019; W. Wang et al., 2016), but to the authors' best knowledge, none of those have simulated the inundation dynamics of both natural river-floodplain systems and manmade-reservoirs over the entire MRB. A recent and notable study by Bonnema and Hossain (2017) used a 0.1° Variable Infiltration Capacity (VIC) model over the MRB to derive time series inflow into some reservoirs. The inundation of individual reservoirs was of interest in their study, hence inundation over other parts of the natural river-floodplain systems was not simulated. Pokhrel, Shin et al. (2018) simulated the natural river-floodplain inundation dynamics over the entire MRB, but the dynamics of inundation caused by existing reservoirs was not considered.

As such, while there is an increasing body of literature on the hydrologic changes in different parts of the MRB, an integrated, basin-wide study that holistically and explicitly simulates the natural and human-induced changes in the flood dynamics is lacking. The present study fills this research and knowledge gap using a newly integrated river-floodplain-reservoir hydrodynamic model. The integrated modeling enables a mechanistic investigation of natural and human-induced changes in surface water dynamics at high-resolution over a large domain, hence providing significant advances to the understanding of Mekong hydrology, especially the impacts of climate variability and dams. We address the following research questions: (1) How have the flood dynamics and surface water storage in the MRB changed over the past four decades? (2) Are the effects of dams significant compared to that of climate variability? (3)

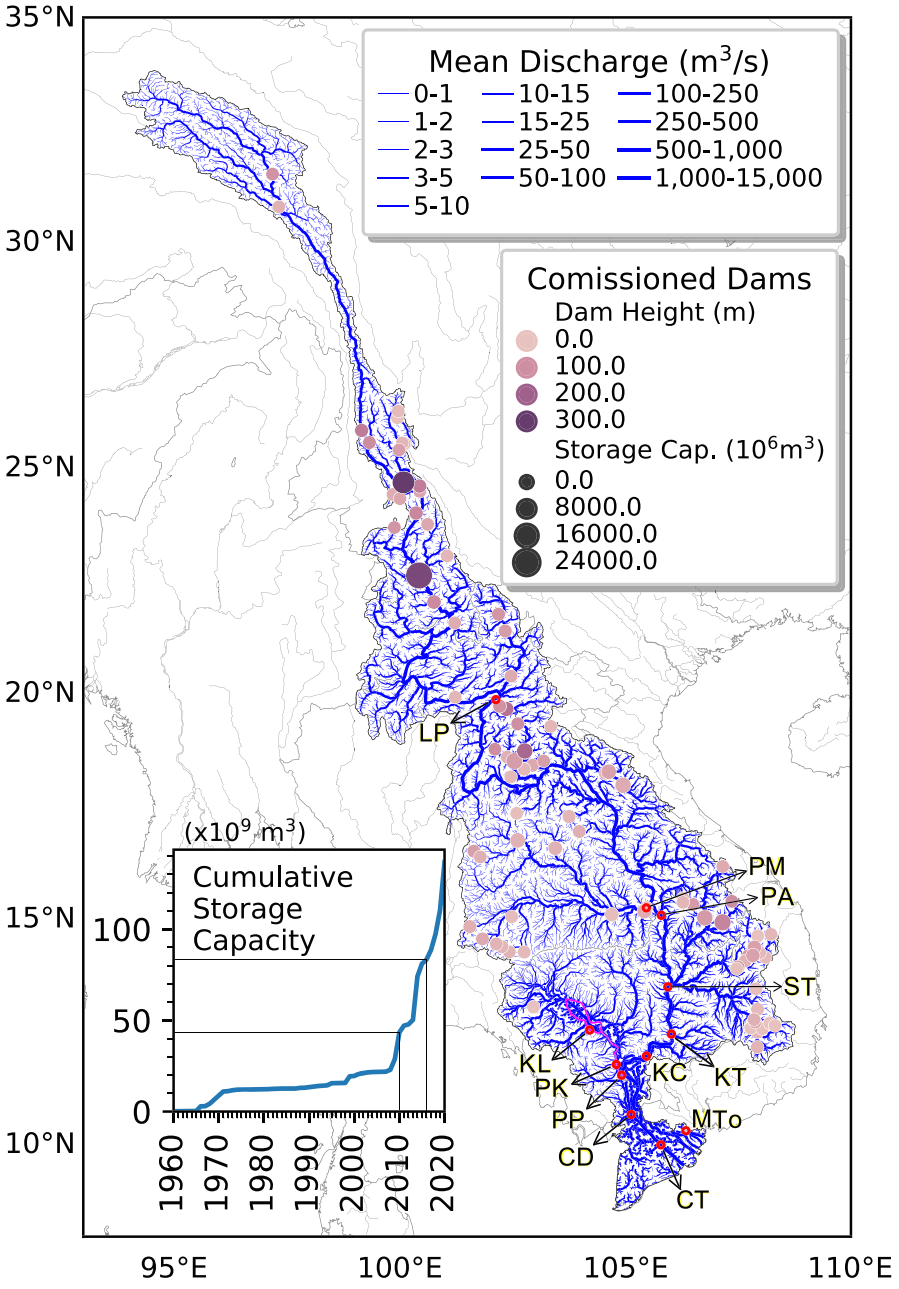

Figure 1. The spatial distribution of river discharge and commissioned dams (as of 2016) over the MRB. The background shows the simulated long-term mean river discharge (1979–2016; 5 km grids). The filled circles show the height (color coded) and storage capacity (circle size) of the 86 selected dams (Table S1). The cumulative reservoir storage capacity from 1960 through 2020 is shown in the lower left inset with indications on the values for 2010 and 2016. The hydrological gauging stations are displayed as red open circles. Station names are: LP (Luang Prabang), PM (Pak Mun), PA (Pakse), ST (Stung Treng), KT (Kratie), KC (Kampong Cham), PK (Prek Kdam), PP (Phnom Penh Port), CD (Chau Doc), CT (Can Tho), KL (Kompong Luong), and MTo (My Tho) (Table S2). Tonle Sap Lake (TSL) and Tonle Sap River (TSR) are indicated by magenta lines.

What will be the potential role of existing reservoirs in modulating surface water storage and inundation dynamics over the MRB in the future? We answer these questions by simulating the historical dynamics of river-floodplain-reservoir storage for the 1979–2016 period, at a spatial resolution of ~5 km. The simulated flood extent is downscaled to a higher resolution of ~90 m to investigate fine-scale inundation dynamics. Such high-resolution modeling is accomplished by integrating a new reservoir scheme (Shin et al., 2019) into a global river-floodplain hydrodynamic model CaMa-Flood (Yamazaki et al., 2013)

version-3.94, resulting in CaMa-Flood-Dam (v3.94). The newly integrated model—which is the first of its kind for the MRB—simulates reservoirs as integral parts of river-floodplain systems at high-resolution and over a large domain (Shin et al., 2019), making it suitable for investigating the changing river-floodplain-reservoir inundation dynamics of the Mekong River system under changing climate and growing dam impacts.

2. Materials and Methods

2.1. Models: CaMa-Flood and HiGW-MAT

CaMa-Flood (Mateo et al., 2014; Yamazaki et al., 2011, 2013) is a global hydrodynamic model, which computes river-floodplain hydrodynamics (i.e., river discharge, flow velocity, water level, and inundated area) by solving shallow water equations of open channel flow, explicitly accounting for backwater effects using the local inertial approximation (Yamazaki et al., 2013). In this study, we use CaMa-Flood version-3.94 that includes major updates to the previous version used in our recent study (Pokhrel, Shin, et al., 2018). The spatial resolution is set to 3-arcmin (5 km) but the simulated flood extent is downscaled to 3-arcsec (~90 m) resolution. For an improved representation of channel bifurcation and the processes therein (Yamazaki et al., 2014)—which are critically important in the LMRB—the maximum number of bifurcation channels is increased from 6 in our recent study (Pokhrel, Shin, et al., 2018) to 10. The previously used SRTM (Shuttle Radar Topography Mission) based DEM (Digital Elevation Model) has been suggested to have multiple errors including absolute bias, stripe noise, speckle noise, and tree height bias (Yamazaki et al., 2017). Here we use the MERIT (Multi-Error-Removed Improved-Terrain; Yamazaki et al., 2017) DEM in which those errors have been resolved such that the stripe-like artifacts in simulated flood extents in low-relief areas, specifically the Mekong Delta (Pokhrel, Shin, et al., 2018), are eliminated. These advancements are essential for a more realistic simulation of river-floodplain dynamics in the MRB. For river-floodplain parameterizations (e.g., flow direction, river-floodplain elevation profile, river length, and river width), MERIT Hydro is used, which is a global hydrography data set based on the MERIT DEM and multiple inland water body data sets (Yamazaki et al., 2019). In addition, a new reservoir extent and release dynamics scheme is incorporated into the modeling framework (details in sections 2.3 and 2.4). We refer to this specific branch of CaMa-Flood that includes the reservoir scheme of Shin et al. (2019) as CaMa-Flood-Dam (v3.94). A complete description of the model physics, parameterization methods, and sensitivities to input parameters in CaMa-Flood can be found in the previous literature (Yamazaki et al., 2011, 2012, 2013, 2014) and the user manual that is available for free download.

CaMa-Flood is driven by runoff from HiGW-MAT (Pokhrel et al., 2015), which is a global hydrological model based on the land surface model called MATSIRO (Takata et al., 2003). HiGW-MAT simulates both the natural water cycle and human activities from canopy to bedrock including evapotranspiration, infiltration, irrigation, flow regulation, and groundwater pumping on a full physical basis. Following our previous study (Pokhrel, Shin, et al., 2018), we use HiGW-MAT in the natural setting (i.e., with human impact schemes disabled) because the objective is to provide runoff as input to CaMa-Flood and reservoirs are simulated within CaMa-Flood (see sections 2.3 and 2.4). The spatial resolution of HiGW-MAT is set to $0.5° \times 0.5°$ (~50 × ~50 km) and the meteorological forcing is taken from the WATCH Forcing Data using the ERA-Interim (WFDEI) database (Weedon et al., 2018). For a complete description of the model physics and parameterizations in HiGW-MAT, readers are referred to the previous literature (Pokhrel, Hanasaki, Koirala, et al., 2012; Pokhrel et al., 2015; Takata et al., 2003). Note that CaMa-Flood can be driven by runoff from any hydrological model. That is, one can use runoff from their own model or freely available global runoff data sets such as those from the Inter-Sectoral Impact Model Intercomparison Project (ISIMIP), which includes runoff from HiGW-MAT.

2.2. Dams and Reservoirs Database

Dam specifications (e.g., location, purpose, year commissioned, height, storage capacity, power generation capacity) are obtained from the database of the Research Program on Water, Land, and Ecosystem (WLE; https://wle-mekong.cgiar.org/), which includes a total of 455 dams (existing, under construction, and planned) within the MRB of which 326 are operational. A comparison of dam and reservoir attributes with the information from other independent sources (e.g., Google Earth, internet resources on individual dams, published literature and reports) revealed that the WLE database contains significant omissions (e.g.,

missing attributes) and discrepancies. For example, of the 326 existing dams, only 80 and 88 include information on storage capacity and height, respectively. Since inaccurate dam specifications can lead to erroneous hydrodynamic modeling, all missing and erroneous specifications should be carefully curated to yield reasonable results for validation against satellite-based datasets such as the Global Surface Water (GSW) data (Pekel et al., 2016).

In this study, the dams that existed as of 2016 (end of simulation period constrained by the availability of WFDEI forcing data; see section 2.6) are imported to the CaMa-Flood modeling framework when they satisfy at least one of the following criteria: (1) dam height $\geq$ 15 m, (2) storage capacity >1 million m^3 (Mm^3), and (3) installed hydropower capacity >100 Mega Watts (MW). The first criterion is commonly used to define large dams (e.g., International Commission on Large Dams (ICOLD); Binnie, 1987; Greathouse et al., 2006; Räsänen et al., 2017). The second criterion is set because it is found from satellite data that the reservoir extents for dams with a storage capacity of <1 Mm^3 and height of <15 m are relatively small, meaning that the upstream inundation caused by these dams could be trivial compared to the model grid size (~5 km). When the first and second criteria are applied, most hydropower dams—even those with installed capacity of <10 MW—are included. However, there were some large dams (in terms of installed capacity) for which dam height and storage capacity were missing, hence we additionally set the third criterion of 100 MW. We fill the missing values from various resources including published reports from the Mekong River Commission (MRC; http://www.mrcmekong.org), Project Design Documents (PDD) provided by Clean Development Mechanism (CDM) of United Nations Framework Convention on Climate Change (UNFCCC) (https://cdm.unfccc.int), documents from construction and design companies, and other peer-reviewed literature. These resources are also used to correct any erroneous records in the dam database. This resulted in the selection of 86 dams for use in this study (Figure 1 and supporting information Table S1).

2.3. Incorporation of Reservoirs Into CaMa-Flood

Importing dams into a grid-based hydrodynamic model requires consideration of two important factors. First, the maximum water depth can be considerably different from the reported dam height due to discrepancies in the database or usage of imprecise and mixed definition of dam height (i.e., dam structure height or the maximum water depth). If the difference is considerably large, the simulated inundation extent corresponding to the reported dam height can be excessive, and vice versa. Second, as discussed in our recent study (Shin et al., 2019), DEM grid elevation represents the water surface level, not the river-reservoir bed elevation. When the preexisting water depth is large, the difference between the actual bed elevation and DEM-based elevation can be too large to be ignored (Shin et al., 2019). Specifically, when large dams are constructed before the DEM is produced, such discrepancies can be huge. The aforementioned issues exist even when a high-resolution DEM (e.g., MERIT DEM) is used. Our examination of the dams in the MRB using two 3-arcsec global DEMs, namely, the MERIT and HydroSHEDS (Lehner et al., 2011), reveals that most reservoirs require considerably lower water depth than their reported dam height to achieve the reported storage capacity (Figure S1). The MERIT DEM shows less deviation from the recorded dam height than the HydroSHEDS DEM (vertical lines in Figure S1), likely owing to more realistic representation of ground elevation by the error correction in MERIT DEM.

When dams are located on the river network of raster model grids, a simple conversion of latitude and longitude into model grid coordinates can cause a mislocation of dams that can lead to erroneous modeling results; for example, some dams in the tributaries can be wrongly located in the mainstem which may cause an unusually high dam inflow and outflow, and vice versa (Shin et al., 2019). Accurately locating dams is also important for realistic representation of inundation patterns since the upstream inundation begins at the dam location. One possible approach is to fine-tune the reservoir location in the model by assuming reservoirs to exist in the grid cell having the most similar upstream drainage area to the known value (Shin et al., 2019); however, reference data for reservoir's upstream drainage area are not available for dams in the MRB. To overcome this limitation, dam locations in the 3-arcsec river network are first determined as the nearest river cells from the given latitude and longitude. Then, the upstream drainage area in 3-arcsec DEM is used as a reference for locating the dams in the 3-arcmin model grid.

Of the 86 selected dams, dam height and storage capacity were missing for nine and 17 dams, respectively. For the 60 dams having both attributes, we find the ratio between the reported dam height and maximum

water depth (i.e., water depth at the dam location to achieve the reported storage capacity) to be ~70% (Figure S2). Accordingly, the maximum water depth for the nine dams is set at 70% of the reported dam height. Finally, the storage capacities of the 17 dams are estimated as the storage when the water level at the dam location reaches 70% of the reported dam height. The inundation extents at those levels are found to be reasonable on visual comparison with the GSW data.

2.4. Reservoir Operation Scheme

The 86 selected dams in the MRB can be classified into three general categories based on their reported purpose: irrigation (22), hydropower (62), and multipurpose (2). We use the reservoir operation scheme of Shin et al. (2019), which determines the seasonality of reservoir release by utilizing water demand in a region, for irrigation dams and employ an optimization scheme to maximize power generation for hydropower and multipurpose dams. Details about the demand-driven scheme can be found in Shin et al. (2019); for completeness, a brief description is provided in the following.

For irrigation dams the release coefficient (K_{rls}[−]), which controls the overall release amount considering interannual variability in storage, is calculated as

$$K_{rls} = \frac{S_0}{\alpha C}, \tag{1}$$

where, S_0 [L^3] is storage at the beginning of the operational year, C [L^3] is the storage capacity, and α is a nondimensional constant set to 0.85 (Hanasaki et al., 2006).

The provisional monthly release (r_m' [L^3/T]) reflecting water demand variability is calculated as

$$r_m' = \overline{i_m} + d_m - \overline{d_m} \quad \text{if } DPI < 1 - M, \tag{2a}$$

$$r_m' = \overline{i_m}\left(M + (1-M)d_m/\overline{d_m}\right) \quad \text{otherwise}, \tag{2b}$$

where i_m and d_m are long-term monthly inflow and demand [L^3/T], respectively. The overbar denotes the annual mean (e.g., $\overline{i_m}$ and $\overline{d_m}$). M is a constant used to ensure $r_m' \geq M\overline{i_m}$, and M is set to 0.1 (Biemans et al., 2011).

Unless reservoir storage falls below the minimum level or exceeds the maximum level resulting in no-release or spill-way release, respectively, reservoir release is set to the targeted monthly release r_m [L^3/T], which is calculated by combining equations 1 and (2):

$$r_m = Rk_{rls}r_m' + (1-R)i_m \quad \text{where } R = \min(1, \alpha c), \tag{3}$$

The minimum water level is set as the level that corresponds to a reservoir storage equaling 10% of the maximum capacity. Because time series data for irrigation demand (d_m) are not publicly available for the MRB, we use the results from HiGW-MAT model as done in Shin et al. (2019). Note that simulated irrigation demand from HiGW-MAT is validated with available country statistics (Pokhrel, Hanasaki, Koirala, et al., 2012; Pokhrel et al., 2015). The reservoir operation scheme described above can also be applied to reservoirs with any other purposes than irrigation if the seasonal water demand for those purposes is available. However, since seasonal water demand or proxy data for hydropower production in the MRB are not available, we use an optimization approach for hydropower dams. Reservoir operation for hydropower can be formulated as an optimization problem that maximizes power benefits, F [$] as

$$F = \sum_{t=0}^{T} P(t)\cdot W(t)\cdot \Delta t = \sum_{t=0}^{T} P(t)\cdot\eta\cdot\gamma\cdot\min(Q(t),\ Q_{turbine})\cdot H(t)\cdot\Delta t, \tag{4}$$

where $P(t)$ is electricity price [$/Watts-hour], $W(t)$ is energy generated [Watts] during the time span of Δt [hr], η is efficiency [−], γ is specific weight of water [kg/m^3], $Q(t)$ is the reservoir release (m^3/s), $Q_{turbine}$ is turbine design flow (m^3/s), and $H(t)$ is turbine head [m]. Since no data are available on $P(t)$, which is a rather complicated function of demand, supply, and numerous other factors (Aggarwal et al., 2009; Weron, 2014), we assume constant $P(t)$ over time. Consequently, the optimization problem is simplified to maximize total

energy production. Such simplification ignores the inundation variability at short time scales (e.g., diurnal and weekly); however, such small-scale variations are expected to be averaged out as the size of the domain (i.e., the entire MRB) and the time scale of interest (i.e., monthly) become large.

In addition to maximizing F, we consider a common practice in hydropower management in which excess water is stored during low-demand and wet periods and released during high-demand and dry periods. Such practice can be formulated in terms of minimizing reservoir storage variation (σ_{STOR}) within a year. In achieving the two hydropower operation objectives, F maximization is assumed to precede σ_{STOR} minimization. That is, after estimating the total turbine discharge (i.e., $\sum_{t=0}^{T} \min(Q(t),\ Q_{turbine})$) that maximizes F, an identical amount is redistributed without additional spillway discharge to minimize σ_{STOR} under the constraints of reservoir storage capacity and time-varying inflow $In(t)$. To reduce the computational cost involved in the optimization that requires iterative hydrodynamic modeling, we employ an approach that utilizes the river discharge simulated without considering dams (Shin et al., 2019). $In(t)$ of a reservoir can thus be estimated as

$$In(t) = \sum_{k=1}^{K} Out(k,\ t) + \left(1 - \frac{\sum_{t=1}^{T}\sum_{k=1}^{K} Out(k,\ t)}{\sum_{t=1}^{T} Q_{NAT}(t)}\right) \times Q_{NAT}(t), \tag{5}$$

where $Out(k,t)$ is monthly outflow of the k-th immediate upstream reservoir at time t, $Q_{NAT}(t)$ is river discharge from the no-dam simulation at the reservoir location and time t, K is the number of immediate upstream reservoirs, and T is the total simulation period. Using equation 5, reservoir release from the uppermost to lowermost reservoirs can be sequentially optimized, first to maximize F, and then to minimize σ_{STOR}.

Information on $Q_{turbine}$ is essential for hydropower optimization, but such information is available only for 12 dams from the data sources listed in section 2.2. An alternative approach is to derive $Q_{turbine}$ from the installed capacity (W_{max}), which is included in the WLE dam database, as $Q_{turbine} = W_{\max}/(\eta \cdot \gamma \cdot H_{\max})$, where H_{max} is the maximum available head. The only available proxy for H_{max} is dam height; however, equating dam height to H_{max} could yield too large $Q_{turbine}$ since, in many cases, turbines are located at lower elevations than dam locations to achieve maximum head (Figure S3). Thus, we employ streamflow with 30% exceedance probability (i.e., Q_{30}) as $Q_{turbine}$, which has been widely adopted in the hydropower literature (Gernaat et al., 2017; Hoes et al., 2017; Zhou et al., 2015). To examine the uncertainty arising from the choice of exceedance probability, sensitivity analysis is performed with simulations that use Q_{20} and Q_{40} as $Q_{turbine}$ (section 2.6). These three flow exceedance probabilities are found to reasonably approximate $Q_{turbine}$ (Figure S4) and are also closely related to the long-term average flow (Figure S5).

No information on operation rules is publicly available for any reservoirs in the MRB; hence, any model development in the MRB has to rely on a generic reservoir scheme that may not fully capture the complex dynamics of real-world reservoir operation. Another challenge is the validation of reservoir release and storage because observed river discharge is generally not available at locations immediate downstream of most reservoirs in the MRB, and storage measurements are entirely lacking. Thus, to deal with the uncertainties in reservoir operation schemes and validation data, we additionally consider two hypothetical hydropower reservoir operation modes, following Piman et al. (2013): full-level and low-level. The full-level operation maintains water up to the maximum level and releases the surplus through turbines or spillway, whereas the low-level operation releases $Q_{turbine}$, which can be Q_{20}, Q_{30}, or Q_{40}, so long as the reservoir water is above the minimum level. These contrasting operation rules at two extremes enable simulations of the probable maximum changes in inundation extent (full-level operation) and river discharge (low-level operation). Conversely, the probable minimum changes in inundation extent and river discharge are simulated by using the low-level and full-level operations, respectively.

2.5. Observed Data and Satellite Radar Products for Model Evaluation

From the observed river discharge and water level data obtained from the MRC, 12 stations are selected that had several years of record for both variables or were located near river confluences (Table S2). To properly locate the observation stations in the 5 km model grids, we utilize the 3-arcsec DEM network, similarly as done for locating dams (section 2.3). For the observed water level obtained from the MRC, no information on the reference datum was available. Thus, to avoid an inconsistent comparison of observed and simulated water levels, the simulated water level for each station is adjusted by including an offset to match the long-term water level during the dry season. For inundation extent, we evaluate the results with Landsat-based GSW data and water body characterization products from Sentinel-1. The regions selected for these evaluations include 37 reservoirs; 19 are the largest reservoirs from three top-10 lists based on dam height, storage capacity, and reservoir extent; and 18 are their neighboring reservoirs (Table S1). To validate the simulated flooded areas over the entire basin, we utilize the aggregated monthly water extent from the satellite composites; specifically, the time series of total flooded areas over the entire MRB from GSW and CaMa-Flood are compared. The spatial resolution of GSW data is 0.00025°, but that of the downscaled CaMa-Flood results is 0.00083° (3-arcsec). Therefore, the comparison with GSW data is presented in two different resolutions: the original resolution and an upscaled resolution of 0.00100°.

The GSW data cover a relatively long period (1984–2018), but since the product is derived from Landsat, it is susceptible to cloud contamination that generally introduces biases in flood occurrence in the wet season. Hence, we additionally use Sentinel-1 (launched in April 2014), which is expected to provide reliable data under all weather conditions. Since the year of 2014 is partly covered by Sentinel-1, we use the data for 2015–2016 (i.e., 24 months) period. Across the LMRB, ~2,000 interferometric wide swath scenes are collected. The processing of Sentinel-1 includes preprocessing (i.e., thermal noise removal, radiometric corrections, coherent speckle noise reduction, and geocorrection) and classification (i.e., unsupervised k-means algorithm and random forest machine learning algorithm) (details in Text S1). To calculate flood occurrence at a pixel, the number of inundated months is divided by the number of data-available months. For comparison purposes, flood occurrence from CaMa-Flood is recalculated for the same period. For a complete description of the Sentinel-1 data processing, readers are referred to the Text S1 and our previous studies (Huang et al., 2018; Torbick et al., 2018).

For a more detailed evaluation, a comparison of flood occurrence between CaMa-Flood and Sentinel-1 is conducted considering land cover types derived from the land cover data provided by the SERVIR Mekong Program (https://servir.adpc.net/), which cover the entire LMRB and are available at 30 m resolution. Since the land use types in 2015 and 2016 were highly similar, we use the data for year 2015. SERVIR data include the following land use categories: surface water, snow and ice, mangrove, closed forest, open forest, other wooded land, settlement, cropland, and wetland. Since the geographic projection and spatial resolution of CaMa-Flood, Sentinel-1, and SERVIR land cover data differ, all products are upscaled to a common resolution of 5 km for a consistent comparison. For this comparison, two subregions of the LMRB are specified: (1) the upper LMRB region (i.e., non-TSL and non-Delta region) and (2) the TSL and Delta region. The dividing point of two regions, as in our previous study (Pokhrel, Shin et al., 2018), is Stung Treng, Cambodia.

2.6. Simulation Settings

First, HiGW-MAT is run for the 1979–2016 period for which the WFDEI forcing data are available. Then, 15 simulations are conducted for the same period but with different settings using CaMa-Flood driven by the runoff from HiGW-MAT. These simulations are categorized into three groups (Table 1): without dams (natural rivers-floodplains; NAT), with dams (individual dams introduced based on historical commission year; DamIND), and with dams (all dams introduced in 1979; DamALL). The historical impact of dams on MRB hydrology is quantified by comparing the NAT and DamIND simulations. DamIND simulations use the reservoir operation scheme of Shin et al. (2019) for irrigation dams and optimized (opt), full-level (full), and low-level (low) operation schemes (details in section 2.4) for hydropower dams. The three hydropower operation schemes are used to provide the upper and lower bounds of uncertainty in reservoir operation. DamIND simulations are grouped into DamIND-opt, DamIND-full, and DamIND-low, and are further detailed according to the setting of $Q_{turbine}$ using Q_{20}, Q_{30}, and Q_{40} to reflect the uncertainty in reservoir operation.

Table 1
Simulation Settings

	Reservoir operation	Irrigation reservoir operation scheme	Start year of reservoir operation	Hydropower reservoir operation scheme	$Q_{turbine}$
NAT	X	-	-	-	-
DamIND-opt-Q_{20}	O	Shin et al. (2019)	Individual dam's historical commission year	Optimized level	Q_{20}
DamIND-opt-Q_{30}					Q_{30}
DamIND-opt-Q_{40}					Q_{40}
DamIND-low-Q_{20}				Low level	Q_{20}
DamIND-low-Q_{30}					Q_{30}
DamIND-low-Q_{40}					Q_{40}
DamIND-full				Full level	-
DamALL-opt-Q_{20}			The start year of simulation (1979)	Optimized level	Q_{20}
DamALL-opt-Q_{30}					Q_{30}
DamALL-opt-Q_{40}					Q_{40}
DamALL-low-Q_{20}				Low level	Q_{20}
DamALL-low-Q_{30}					Q_{30}
DamALL-low-Q_{40}					Q_{40}
DamALL-full				Full level	-

While the DamIND simulations are used to investigate how reservoirs have affected historical surface water dynamics in the MRB (Questions 1 and 2), DamALL simulations are used to quantify the potential future impacts of existing reservoirs (Question 3). Hence, the settings for DamALL simulations are almost identical to those for DamIND simulations; the only difference is that in the DamALL simulations all 86 dams are assumed to have existed from 1979. That is, in DamALL simulations the operation of all 86 dams begins in 1979 regardless of the historical commission year of individual dams, thus enabling the assessment of their potential future impacts on flood dynamics under business-as-usual conditions. Thus, the DamALL simulations enable inference on the potential future impacts of existing dams under the assumption of historical climate and no future dams.

3. Results and Discussion

3.1. River Discharge and Water Level

Figure 2 presents the evaluation of simulated river discharge at seven selected stations (Table S2) in the mainstem and tributaries of the Mekong. The spatial distribution of the long-term (1979–2016) mean is shown in Figure 1. Figure 2 provides seasonal cycles for seven different periods. First, results are presented for the 1979–2009 and 2010–2016 periods (Figures 2a and 2b); year 2010 is chosen to divide the two periods since the total basin-wide reservoir storage capacity doubled in that year compared to its preceding decades (Figure 1 inset). Daily time series for two dry years (1998 and 2015) and two wet years (2000 and 2011) are then presented along with the available observations (Figures 2c–2f). Finally, the last column shows the seasonal cycle for all years for which observations are available. Further, a complete time series is provided in the supporting information (Figures S6). Performance metrics (i.e., correlation coefficient and root-mean-square error) are presented for the NAT and DamIND simulations in Table S3.

The NAT and DamIND simulations show similar seasonal patterns and comparable performance as the relative difference in performance metrics are mostly <5% (Table S3). Evidently, the long-term variability in river discharge and its seasonal cycle in the main stem Mekong (Figures 2 and S6; LP, PA, ST, KT, KC, and PP) and a tributary (PM), as well as the TSR flow reversal (PK), are accurately reproduced by the model. In the Delta region (CD and CT) where the Mekong flow diverges into several distributaries, some differences in low- and high-flows are evident between the observations and simulations, which could be partly because of imperfect channel bifurcation parameterizations and partly due to missing tidal effects in the model. Overall, we find the results to be acceptable given the scale of the model domain (i.e., the entire MRB), uncertainties in available data, and difficulty in accurately representing channel bifurcation process.

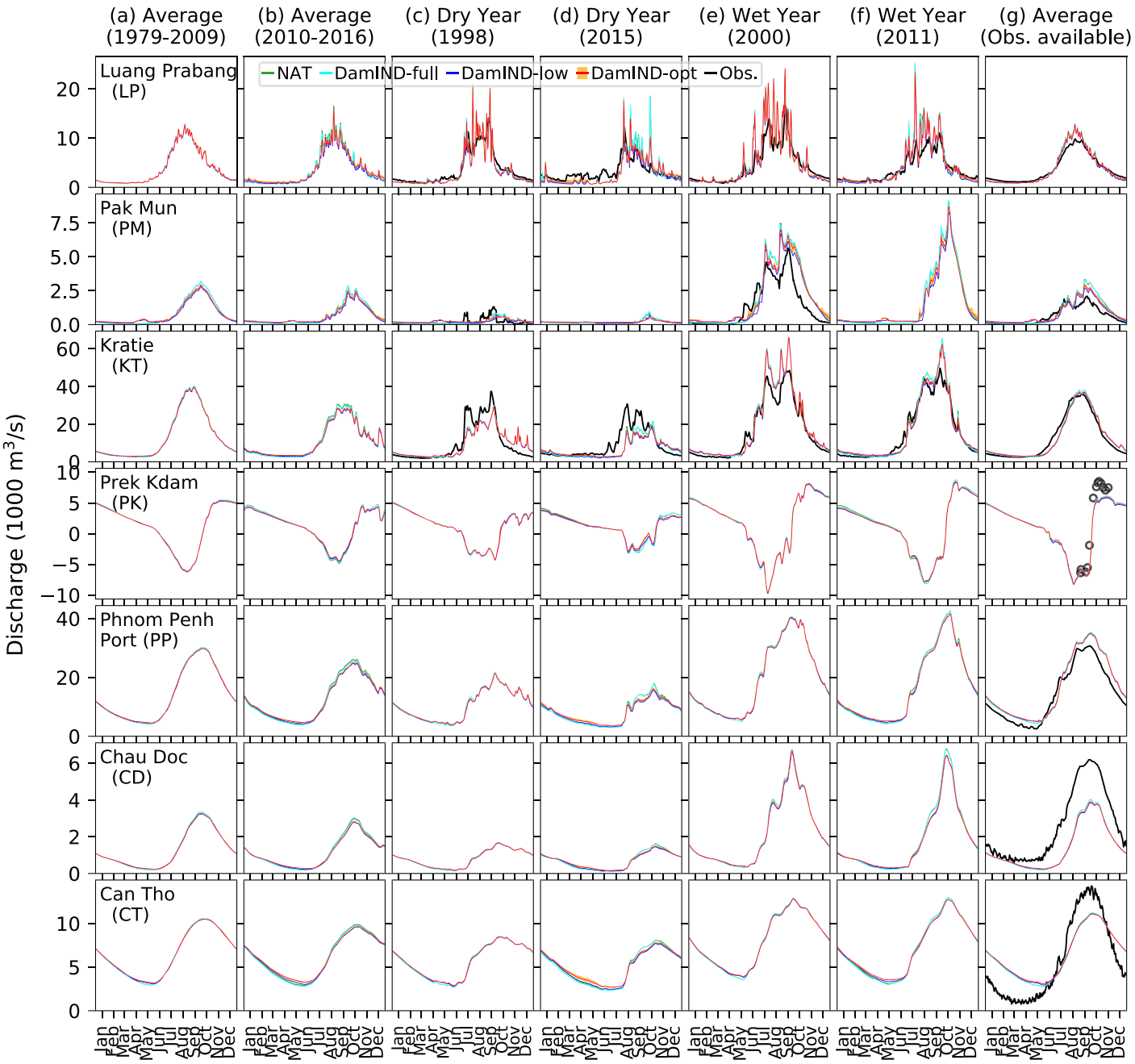

Figure 2. Validation of simulated river discharge. Seasonal average for the periods of (a) 1979–2009 and (b) 2010–2016, (c–f) daily time series for and dry- and wet-years, and (g) seasonal average for the period when observation (Obs.) is available are presented. The complete daily time series for all stations and the observation available period are presented in the ;supporting information (Figure S6). The orange shading indicates the level of uncertainty in the optimized hydropower operation. The locations of stations are shown in Figure 1.

Simulated water level shows a close match with observation (Figures 3 and S7); that is, simulated water levels in the main stem Mekong (LP, PA, ST, KT, KC, and PP stations) are in close agreement with observations. However, seasonal dynamics are not fully captured at locations in the Delta region (CT and MTo) where the high-frequency fluctuations in observations—likely caused by tides—are not captured by the model. Ikeuchi et al. (2017) noted that the incorporation of tidal effects could improve the simulation of water level near the ocean, even though the effects were found to be small (<0.2 m) due to relatively large river flows from the upstream compared to tides and surges. For the TSL, water levels are reproduced

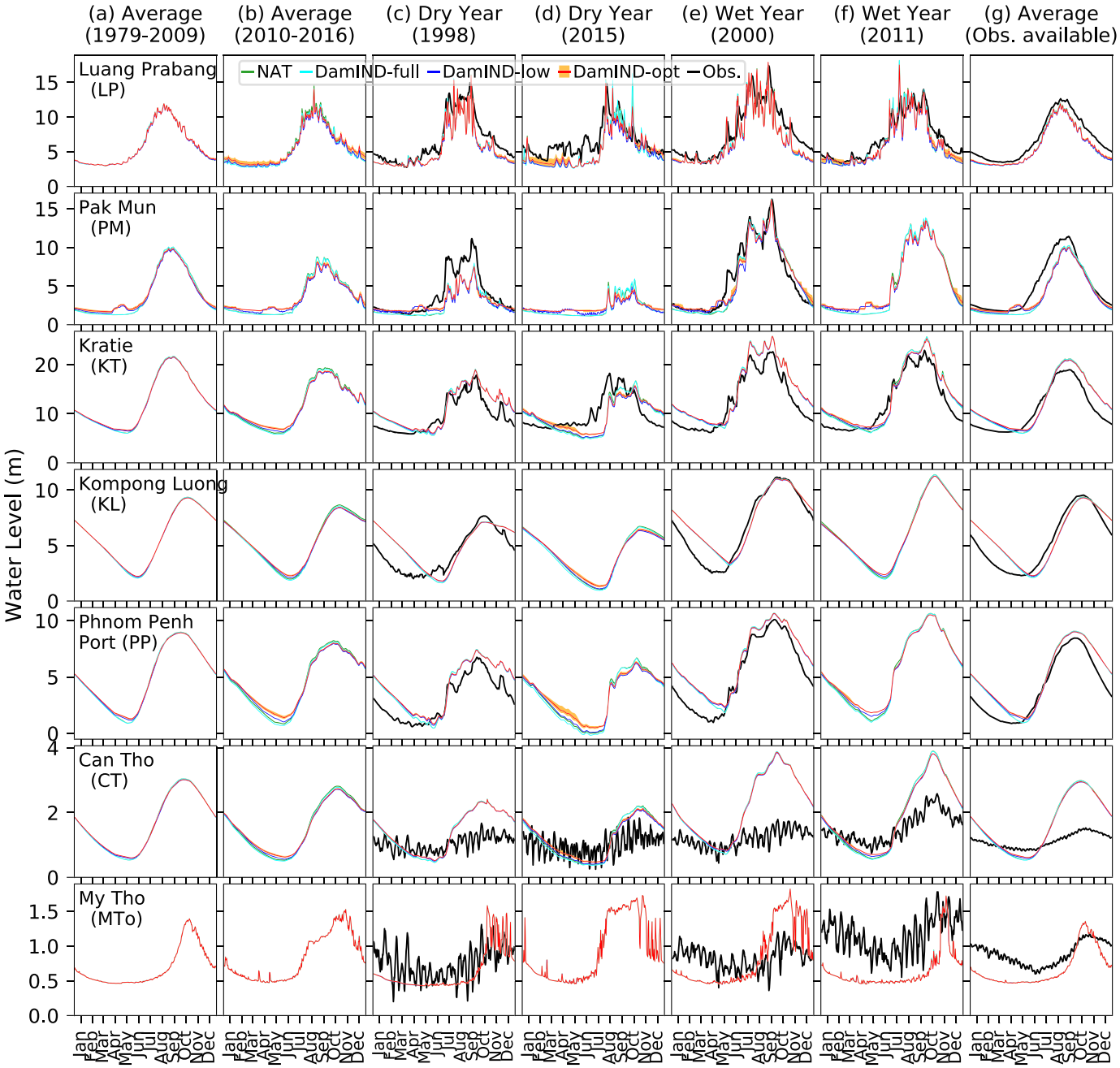

Figure 3. Same as in Figure 2 but for water level. The complete daily time series for all stations and the observation available period are presented in the supporting information (Figure S7).

remarkably well (Figure 3). That is, water levels within the lake (KL station) and at the confluence of TSR with the Mekong (PP station) both agree very well with observations, suggesting that the TSR flow reversal—which is driven by water levels at PP and the lake—is accurately represented in the model. Overall, the results suggest that the seasonal dynamics of a complex fluvial system can be accurately simulated with the dynamic wave equation used in CaMa-Flood. Meanwhile the discrepancies in the Delta region underscore the need for improved channel bathymetry and bifurcation parameterizations and for including tidal effects in the model. However, in terms of monthly variability of inundation extents, which is closely related to water level, tidal effects at submonthly scale can be expected to be

averaged out. Moreover, since such biases are inherent in all simulations, the tidal effects on difference between two simulations (e.g., NAT and DamIND) used to assess dam impacts are minimal.

To investigate the historical impact of climate variability and reservoirs on the dynamics of river flow and water level, we compare the NAT and DamIND simulations. Large interannual variations in peak and low flows are evident in the NAT simulation, in which reservoirs are not considered (Figures 2 and 3). When reservoirs are considered (DamIND), peak and low flows are dampened. The differences between the NAT (green in Figures 2 and 3) and DamIND (cyan, blue, and red with orange shades in Figures 2 and 3) simulations indicate the degree of reservoir impact on river flow and water level; evidently, the impact has increased monotonically over time becoming greatest in recent years (e.g., 2010–2016; Figures 2b and 3b). Despite the monotonic increase in reservoir impact, compared to changes in discharge and water level due to climate variability, reservoir induced variability is found to be small (e.g., NAT vs. DamIND) even when uncertainties in reservoir operation are considered (e.g., differences among DamIND simulations). Results suggest that reservoir operation has exerted limited influence on the variations of discharge and water level during the 1979–2009 period (Figures 2a, 3a, S6, S7), except for the Mun river basin (PM station) where many reservoirs were built before or early in the simulation period. These results clearly indicate that climate variability has dominantly modulated flood dynamics in the MRB in the past four decades, and that the impacts of dams were marginal until 2009.

Nonetheless, as more dams are built (e.g., Nuozadu, Xiaowan, Xe Kaman, and Nam Ngum 1; Table S1) with the basin-wide storage capacity doubling in 2010, the effects of reservoir operation on river flow and water level have become more pronounced. This is discernible during the 2010–2016 period (Figures 2b and 3b; difference between NAT and DamIND simulations). In this period, the dam-induced changes in peak flow, low flow, and seasonal amplitude (i.e., maximum-minimum flow) at the LP station were −5%, 22%, and −6%, respectively (comparison of NAT and DamIND-opt; Tables S4). The same effects during 1979–2009 period were 0% for all three aspects (Table S4), which clearly suggests that there is an increase in the effects of dams in recent years. The increasing reservoir effects are found in both dry and wet years at all stations (Table S4). Specifically, dams influenced both the normal and reverse flows in the TSR (PK station) during 1979–2009 period by −2%. The same effects were greater during 2010–2016 period (i.e., −5% and −9% for normal and reverse flows, respectively), and more so during the dry year of 2015 (i.e., −8% and −12% for normal and reverse flow, respectively). These results corroborate our previous findings about changes in open water areas in and around TSL during the same period (Lin & Qi, 2017).

Results from the DamALL simulations (see section 2.6) suggest that potential future dam impacts could be considerably larger than today, even under the historical climate and no additional dams (Figure 4; Figures S8 and S9; Table S5). Both river discharge and water levels could be substantially altered by the existing reservoirs. For example, existing reservoirs could potentially alter the peak flow, low flow, and seasonal amplitude of the climatological daily seasonal cycle at the LP station by −11%, 58%, and −16%, respectively (comparison of NAT and DamALL for 1979–2016 period; Table S5). In the TSR, the rate of normal (reverse) flow could change by −6% to −10% (−13% to −16%) in dry years, −4% to −5% (−4% to −7%) in wet years, and −7% (−9%) during average years. Note that identical climate condition and reservoir operation schemes are used for DamIND and DamALL simulations, but the potential future impacts of existing dams (i.e., DamALL) are considerably greater than their historical impacts (i.e., DamIND).

Overall, our results show that seasonal dynamics and interannual variations in river flow and water level in the MRB were governed primarily by climate variability until the 2000s. However, the effects of dams increased significantly from 2010 onward, and it is expected that even under business-as-usual conditions, dams could profoundly alter the future flood dynamics. Further, these effects could be largely compounded by future dams and climate change; however, as evident from the uncertainty range in Figures 2–4 and S6–S9 and Tables S4–S5, future impacts will depend on how reservoirs are operated.

3.2. Spatial Pattern of Long-Term Flood Occurrence

Figure 5 presents the 3-arcsec (~90 m) grid flood occurrence (i.e., flood frequency in percentile) over the entire MRB for the 1979–2016 period, which is derived from the downscaled monthly average flood depth simulated by CaMa-Flood at ~5 km resolution. Comparisons with the GSW data are provided in Figure 6 and in the supporting information (Figure S10). A similar comparison using the Sentinel-1 products is

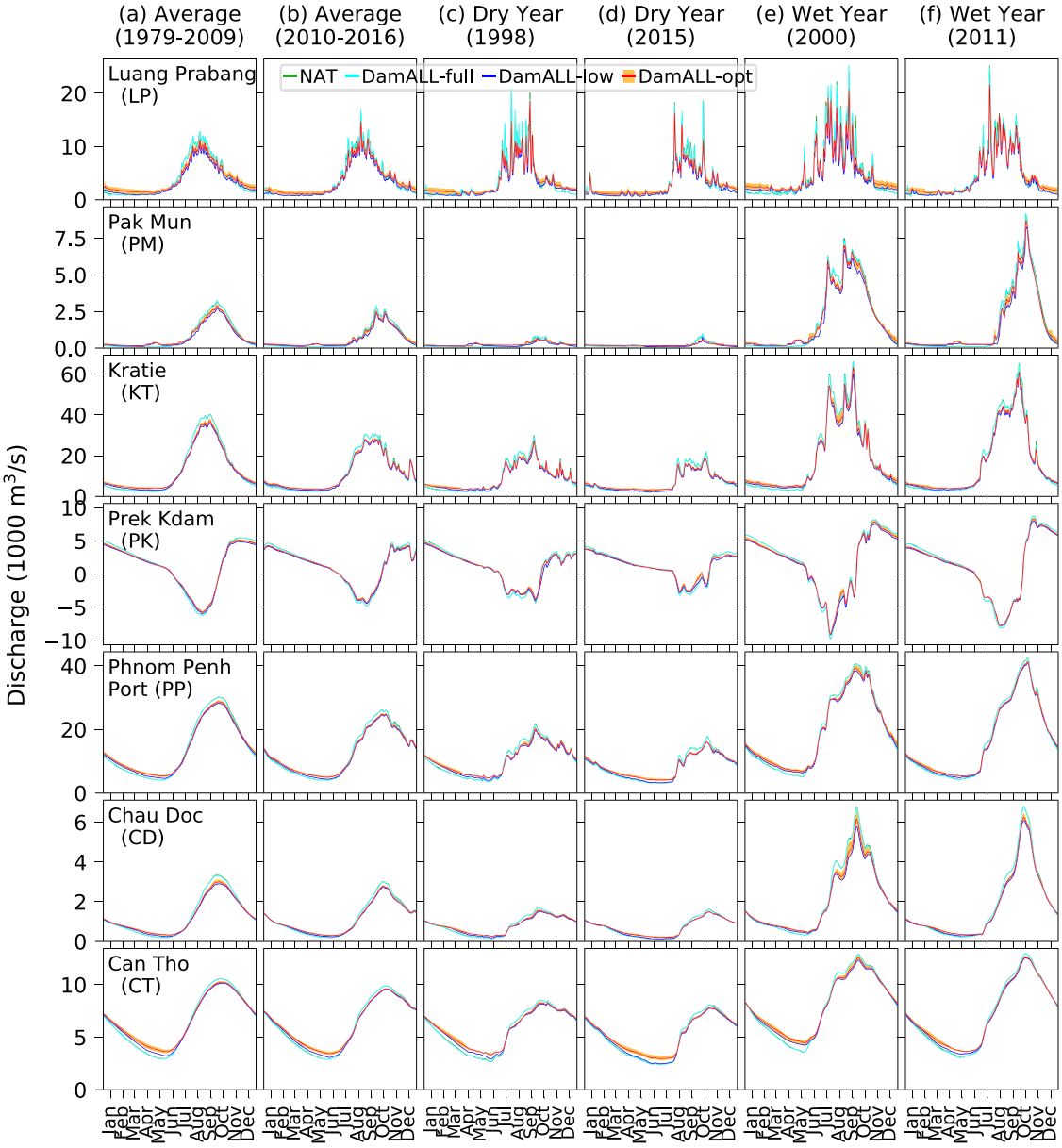

Figure 4. The potential impacts of 86 existing dams on river discharge estimated from the DamALL simulations. Figure format is the same as in Figure 2, except for the observation, which is excluded here since the results are for DamALL simulations. The complete daily time series of river discharge and water level for all stations are presented in the supporting information (Figures S8 and S9).

presented in Figure S11. The model captures the broad spatial patterns of flood occurrence seen in the GSW data and Sentinel-1 for both natural river-floodplain-lake systems and manmade reservoirs (Figure 6). The permanent water body in the TSL is accurately simulated by CaMa-Flood to be always flooded (Figure 6a left panel; dark blue; 100% flood occurrence). As also noted in Pokhrel, Shin et al. (2018), the GSW data do not suggest such permanent flooding, a potential issue in the Landsat product (Figure 6a right panel). Meanwhile, Sentinel-1 suggests permanent flooding in the lake (Figure S11), which shows the potential of the Sentinel-1 for resolving flooded areas in cloud-prone seasons (Bouvet et al., 2009; Nelson et al., 2014; Torbick, Chowdhury, et al., 2017; Torbick, Salas, et al., 2017).

Further, variations from the center of the lake to its largest outer extent are smooth and continuous in CaMa-Flood results, while those variations seem rather abrupt and, often, nonexistent (i.e., no flooding;

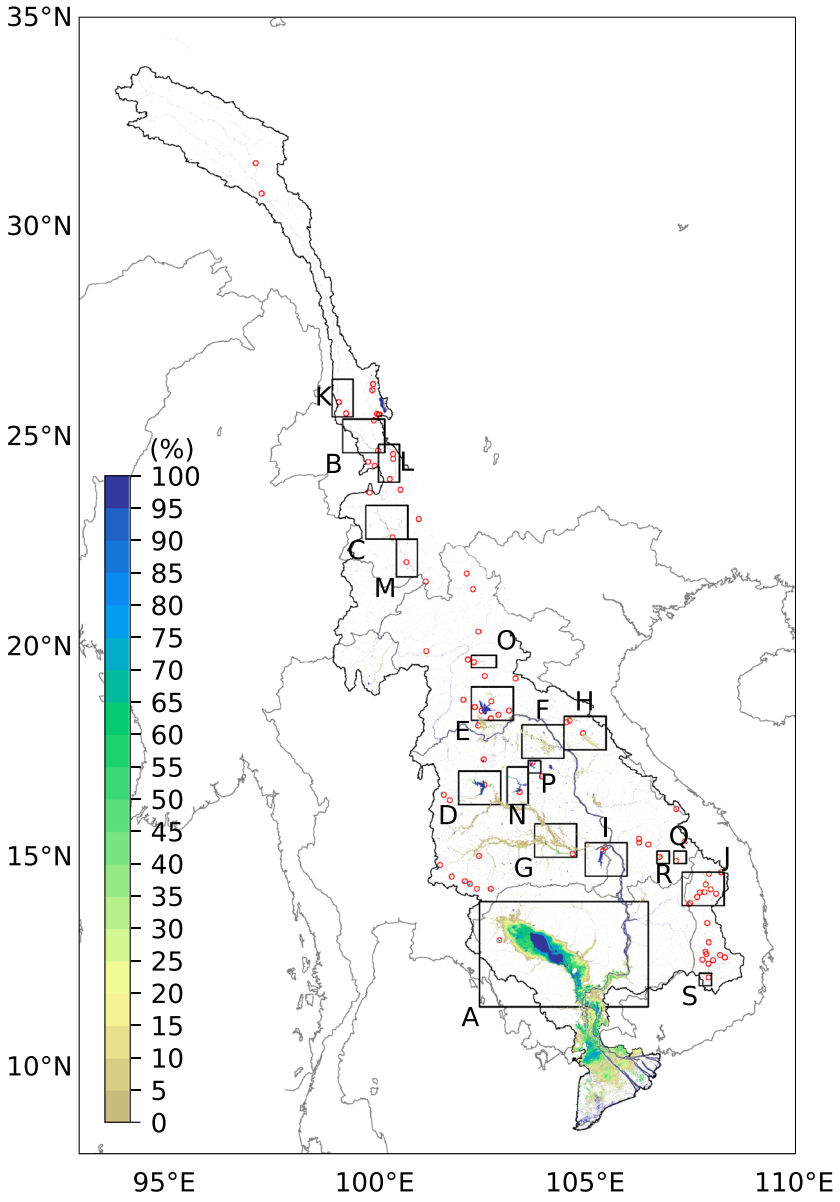

Figure 5. Simulated flood occurrence at 3-arcsec (~90 m) resolution for the entire MRB. Black boxes indicate the regions used in Figure 6 for the validation of simulated spatial inundation dynamics. Red circles indicate dam locations.

areas in white in Figure 6a right panel) in the GSW data. Sentinel-1 also exhibits similar patterns of flood occurrence around the lake as in the GSW data (Figure S11). Such patterns in both satellite products could be attributed to the underestimation of flooded areas since those area are mostly forested floodplains (e.g., gallery forest and flooded shrubland) (Arias, Cochrane et al., 2014), where vegetation interferes with both optical and radar sensors. For the reservoirs, the spatial patterns of the maximum inundation extent seen in the GSW data are reproduced remarkably well by CaMa-Flood (Figures 6b–6e; 6h–6s). Note that the uncertainties in GSW data for manmade reservoirs are expected to be minimal compared to that for natural water bodies (e.g., the TSL) because of clearly distinguishable open water surface. A good agreement between the simulated maximum water extent and GSW data also ensures that the uncertainties in reservoir attributes (e.g., dam height and storage capacity) have been minimized in our data processing (sections 2.2 and 2.3); that is, any erroneous dam specifications could have resulted in misrepresentation of the inundation patterns in the upstream of the reservoirs.

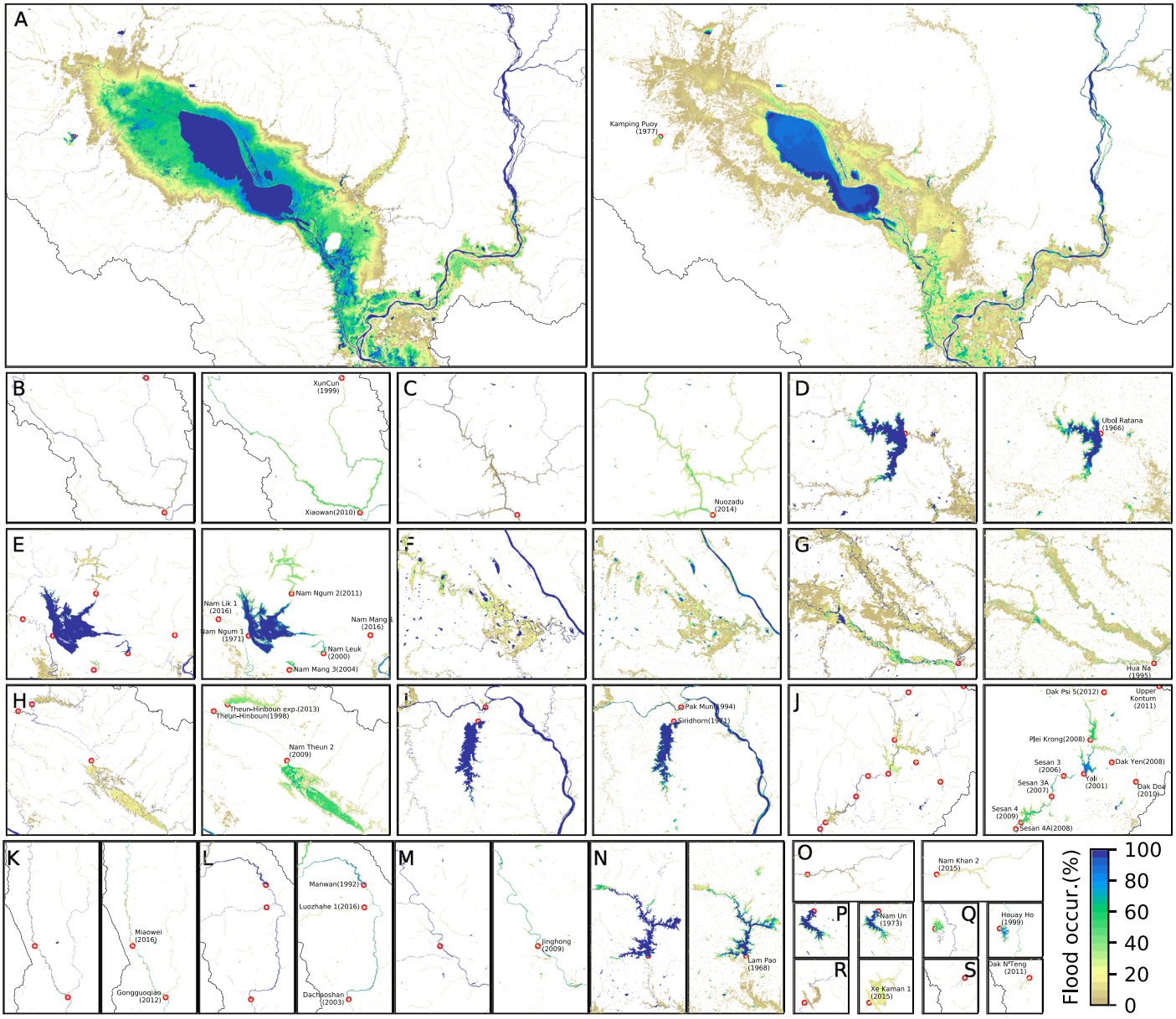

Figure 6. Spatial validation of simulated inundation dynamics. Simulated flood occurrence (left; CaMa-Flood) for 1979–2016 is compared with the GSW flood occurrence (right; Pekel et al., 2016) for 1984–2018 period. The locations of sub-panels from A to S are shown in Figure 5. Red circles indicate dam locations. The resolution of GSW flood occurrence is 0.00100°.

In terms of inundation patterns within the reservoirs (e.g., Xiaowan, Nuozadu, and Nam Ngum 2 in Figures 6b, 6b, 6e, respectively), differences can be seen even for the reservoirs discussed above, due to several reasons. For both satellite products, as mentioned above, underestimation in flood occurrence is expected because of the interference effect (e.g., clouds, debris, and vegetation cover). Specifically, the number of cloud-free images from Landsat is limited in the monsoon season (Figure S12), which could have caused an underrepresentation of flood occurrence in the GSW product. Additionally, the discrepancy between the GSW data and the model could be caused partly by the use of different time periods between the two (CaMa-Flood: 1979–2016; GSW data: 1984–2018); however, the uncertainties from this mismatch are marginal compared to those caused by missing records in the GSW data (Figure S12). For Sentinel-1, the short time period (24 months) used in calculating flood occurrence can be a cause of uncertainty. Further, uncertainties in meteorological forcing could have impacted CaMa-Flood simulations partly

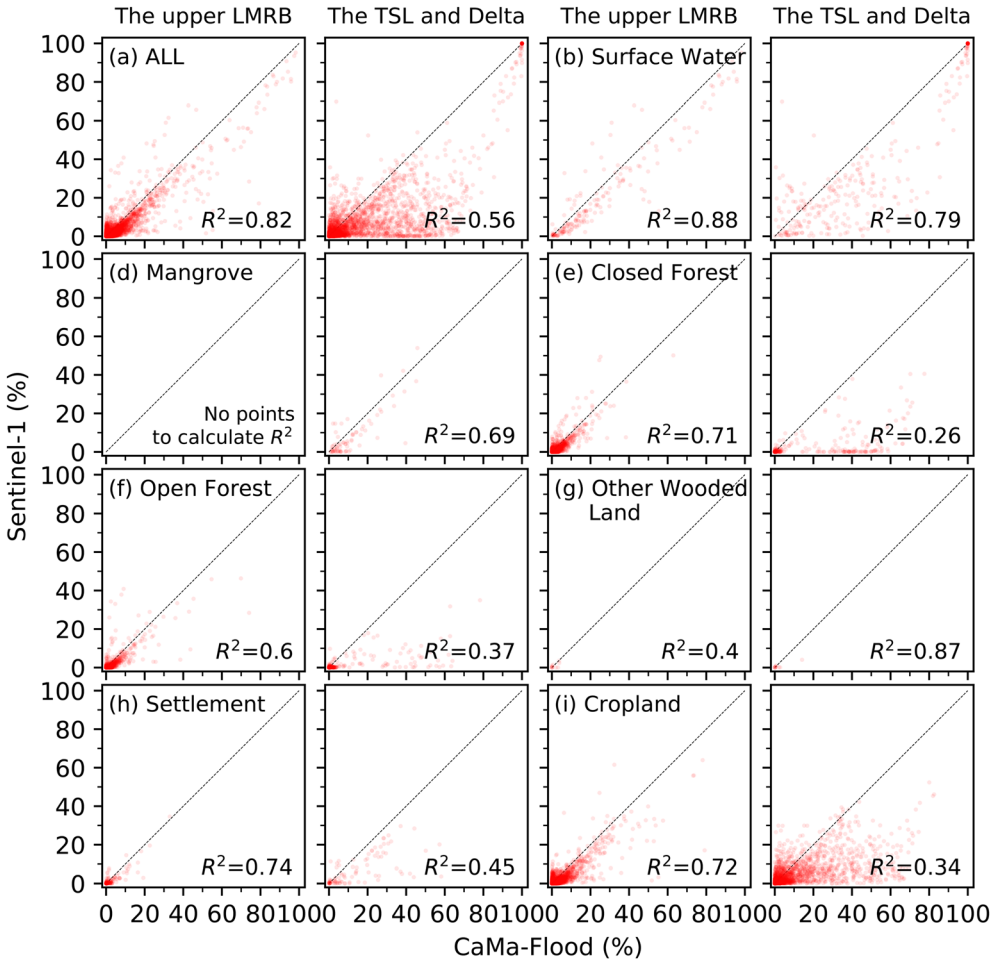

Figure 7. Comparison of CaMa-Flood and Sentinel-1 based flood occurrences for different land cover classes. The paired sub-panels for (a) all classes and (b-i) each class are for the upper LMRB (left) and the TSL and Delta (right) regions. The dotted black diagonal lines represent 1:1 lines.

contributing to the differences, but good agreement between the simulated and observed discharge and water level (Figures 2 and 3) provides confidence that the effects of uncertainties in forcing are minimal. Imperfect topography data could have introduced additional uncertainty in the model; while many errors and noises have been removed in the MERIT DEM (Yamazaki et al., 2019, 2017), the water body within the reservoirs that existed when the SRTM (primary data source for MERIT DEM) was launched (February 2000) is still a potential source of error. In general, the DEM values over the reservoirs built before the launch of SRTM tend to be flat, causing dampened seasonal variation in reservoir extent in CaMa-Flood compared to that in GSW data for the reservoirs built prior to year 2000 (e.g., Ubol Ratana, Nam Ngum 1, Siridhorn, Lam Pao in Figures 6d, 6e, 6i, and 6n, respectively).

Upstream inundation begins exactly at the location of the dam, but a dam can be located at any point within the 5 km modeling grid. Thus, when flood occurrence is downscaled to ~90 m grids, the location where inundation begins in the downscaled results may not perfectly match the actual dam location. For example, inundation begins at a location slightly downstream (e.g., Nuozadu, Miaowei, and Nam Khan 2 in Figures 6c, 6k, and 6o, respectively) or upstream (e.g., Theun-Hinboun exp., Yali, and Manwan in Figures 6h, 6j, and 6l, respectively) of the dam location. This is unavoidable in grid-based reservoir modeling, but the errors can be minimized by increasing the spatial resolution. Additionally, the spatial variations in inundation extent for reservoirs built before the SRTM launch can be better simulated by using improved reservoir bathymetry data where local information is available (Busker et al., 2018; Li et al., 2019; Shin et al., 2019; van Bemmelen et al., 2016).

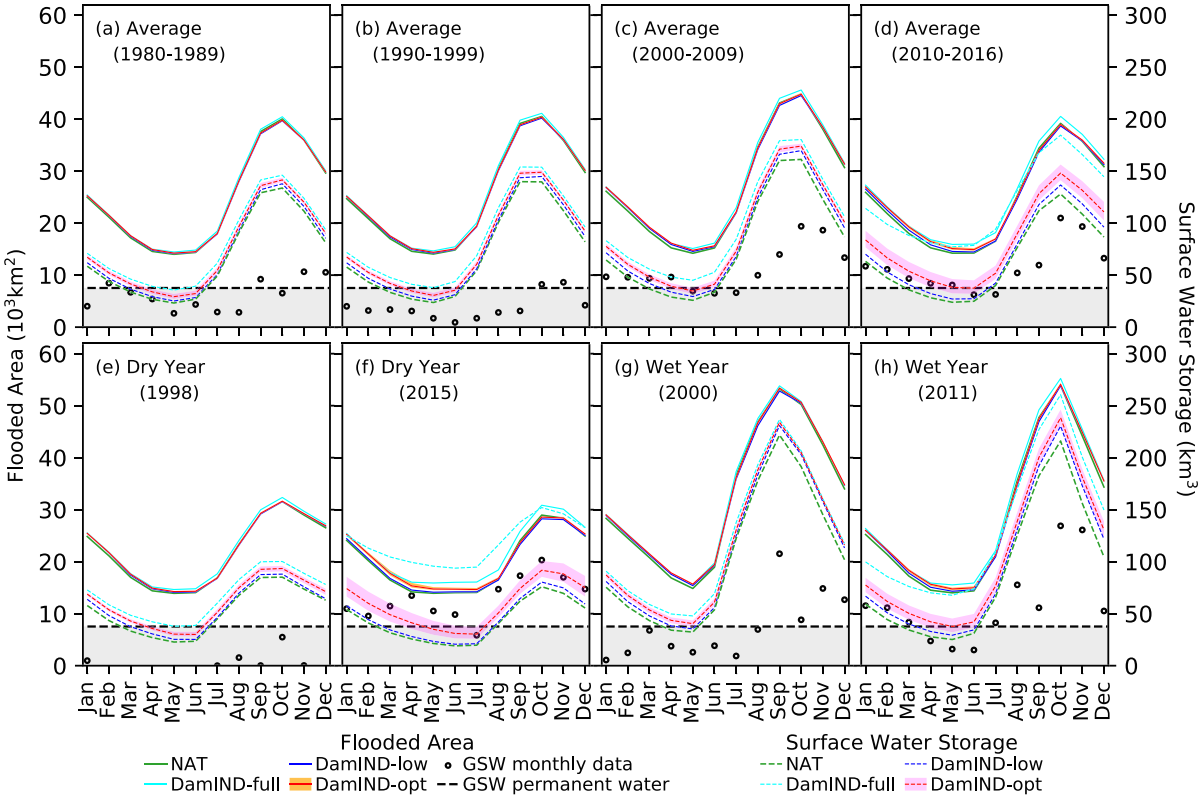

Figure 8. Historical flooded areas and surface water storage dynamics over the MRB. The seasonal average and monthly time series are presented for (a–d) the selected periods and (e–h) dry- and wet-years. The orange and pink shadings indicate uncertainty range in the optimized hydropower operation for flooded areas and surface water storage, respectively. The monthly GSW flooded areas for 1984–2016 is presented for the periods and years wherever available. The black dotted lines with gray shades indicate the permanent water areas in the GSW data.

3.3. Dependence of Flood Occurrence on Land Cover

Flood occurrence from CaMa-Flood shows good agreement with the Sentinel-1 data for most land cover types (Figure 7). Differences between the two are found to be smaller in the upper portion of the LMRB than in the TSL and Delta region, likely because of the steeper relief in the upper LMRB that enables the inundation patterns to be more distinctively confined by the local topography. In the TSL and Delta region, flood occurrence in Sentinel-1 data is less than in CaMa-Flood, specifically for the forested areas surrounding the TSL (Figure S11). Considering that the saturation of C-band Sentinel-1 is limited for dense vegetation canopy at high biomass levels (El Hajj et al., 2019; Hess et al., 1990; Huang et al., 2018), we conclude that Sentinel-1 underestimates flood occurrence in forested areas around the lake. For densely vegetated regions, L-band remote sensing products can be potentially more useful (Urbazaev et al., 2018); however, open access, operational, and high temporal frequency L-band data over large regions do not exist at this time. The notable differences for areas with human settlement and cropland can be attributed to an overestimation in CaMa-Flood owing to missing water infrastructure such as levees. The incorporation of such flood control infrastructure can result in less frequent simulated inundation.

3.4. Flooded Areas and Surface Water Storage

Figure 8 presents the seasonal dynamics of surface water storage and flooded areas based on the decadal (Figures 8a–8d) mean of CaMa-Flood simulations and GSW monthly flooded areas over the entire MRB. The seasonal variabilities for selected dry (1998 and 2015) and wet (2000 and 2011) years are also shown (Figures 8e–8h). The results for the entire simulation period of 1979–2016 are presented in supporting information (Figure S13). CaMa-Flood results indicate that basin-wide flooded areas account for 3–7% (28,000–54,000 km^2) of the basin area in the wet season and <2% (14,000 km^2) in the dry season.

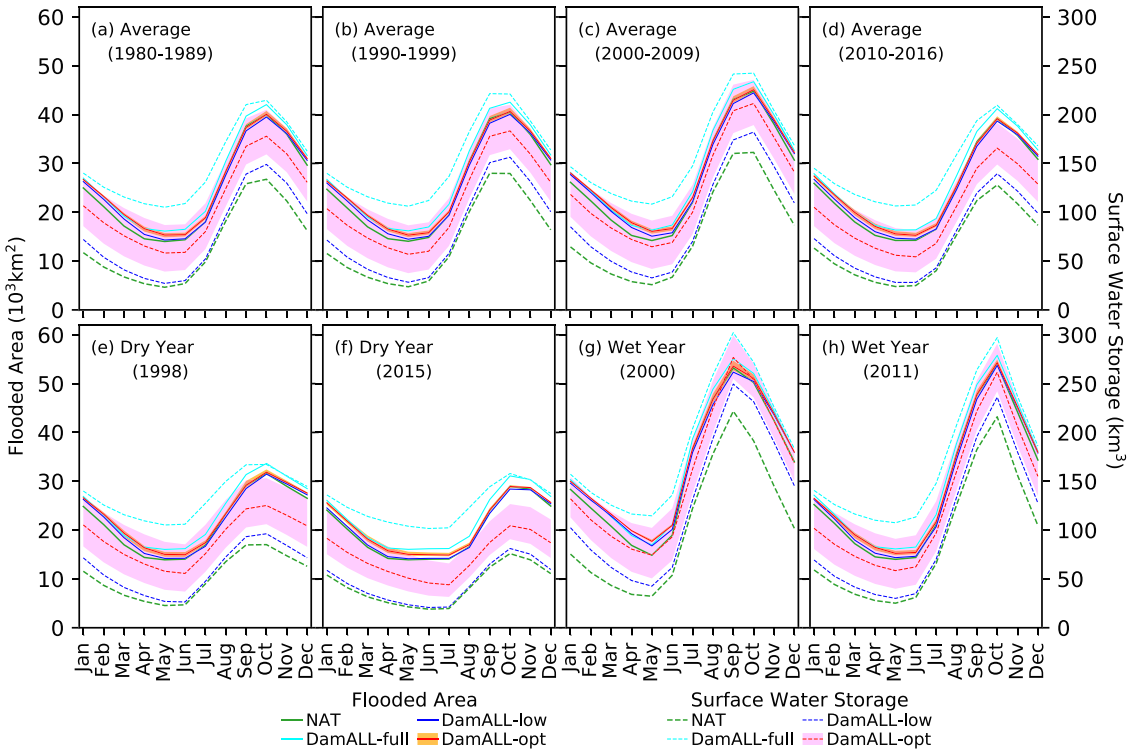

Figure 9. The potential impacts of 86 existing dams on surface water dynamics estimated from the DamALL simulations. The seasonal average and monthly time series are presented for (a–d) the selected periods and (e–h) dry- and wet-years.

Differences are evident between the flooded areas in CaMa-Flood results and GSW data, specifically before the 2000s and the flooding season (Figures 8 and S13). As discussed in section 3.2, the mismatch could be partially attributed to the model overestimation, mainly due to uncertainty in the DEM and an underestimation in the GSW data, due to vegetation, cloud, and missing records. A detailed inspection of the GSW product reveals that >45% of the area in the MRB has pixels classified as "No Data" for at least a month in each year, and the annual average of "No Data" pixels is >49%, specifically for years before 2002 (Figure S12). In addition, total flooded areas in the GSW data increase after 2002, which is accompanied by a reduction in the number of months with "No Data" pixels (Figures S12–S13), further suggesting that the flooded areas could have indeed been underestimated heavily for the pre-2002 period. The effect of "No Data" pixels is also evident when the GSW monthly time series is compared to the GSW permanent water areas, which are portions of river, lakes, and reservoirs that have been permanently covered by water during the 1984–2018 period. The GSW data suggest the permanent water areas over the MRB—the minimum value in the GSW monthly time series—to be 7,530 km^2 (black dotted lines in Figures 8 and S13), but the GSW monthly time series numbers are far below that minimum area due to significant missing values.

While the interannual variability is evident in the surface water storage and extent dynamics, no significant interannual trend is found in the NAT simulation for the minimum, maximum, mean, standard deviation, and the maximum amplitude of flooded areas (Figures 8 and S13; Mann-Kendall test, $p > 0.26$ for all variables, $\alpha = 0.05$; hereafter only the maximum and minimum p-values are provided where trends exist and do not exist, respectively) and surface water storage ($p > 0.39$). All DamIND simulations, except for DamIND-low-Q_{20}, which is designed to provide the lowest bound for the impacts of dams on flooded areas and water storage (section 2.6), indicate increasing trends in the minimum flooded areas and minimum surface water storage ($p < 0.02$). Meanwhile, none of the DamIND simulations shows significant trends in standard deviations and the maximum amplitudes ($p > 0.61$). These results indicate overall that reservoirs have influenced surface water storage and extent dynamics in the dry season while climate variability has dominated the wet season interannual variations in surface water storage and extent dynamics.

Two dry years (i.e., 1998 and 2015) are similarly dry in terms of river discharge (Figure 2), but the historical impact of reservoirs is evidently higher in 2015 than in 1998 since the total number and storage capacity of reservoirs in 2015 increased by more than fivefold and twofold, respectively, from 1998 (Figures 8e and 8f). Meanwhile, those two dry years show similar reservoir impacts in DamALL simulations since the number of simulated reservoirs is the same throughout the entire period (Figures 9e and 9f). As such, the DamALL simulations show no significant trends in either flooded areas or surface water storage for any of the attributes of the minimum, maximum, mean, standard deviation, and the seasonal amplitude ($p > 0.12$). We note that these results should be interpreted with caution since the outcome could vary if additional dams are considered or if climate projections having wetter or drier trends are used as input forcing. Compared to the DamIND simulations, the DamALL simulations show higher deviations from the NAT simulation, and larger variabilities in surface water storage and extent dynamics over the entire simulation period (Figures 9 and S14). The considerable differences between the DamIND and the DamALL simulations suggest that surface water storage and extent dynamics in the future could be largely different from that in the past even under business-as-usual conditions.

4. Summary and Conclusion

In this study, the historical dynamics of river-floodplain-reservoir storage and extent over the entire MRB is simulated for the 1979–2016 period and at a high-resolution (3-arcmin; ~5 km). The simulated flood extent is further downscaled to 3-arcsec (~90 m) grids to investigate the changes in fine-scale inundation dynamics. Integrated modeling of natural river-floodplain and reservoir (86 that existed as of 2016) systems is accomplished with the incorporation of a recently developed reservoir scheme (Shin et al., 2019) into the global river-floodplain hydrodynamic model CaMa-Flood (Yamazaki et al., 2013) version-3.94, resulting in CaMa-Flood-Dam (v3.94). Reservoir operation is simulated using a demand-driven scheme (Shin et al., 2019) and an optimization-based operation scheme for irrigation and hydropower dams, respectively. The natural and human-induced changes in flood dynamics over the entire basin are investigated simultaneously using this newly integrated modeling framework. Results are validated with ground-based observations for discharge and water level, and remote sensing products (the GSW and Sentinel-1 data) for spatial inundation dynamics. Uncertainties in reservoir operation are quantified using three different turbine design flows (Q_{20}, Q_{30}, and Q_{40}) and a range of operation modes (opt, low, and full) (section 2.6 and Table 1). Results from simulations with (i.e., DamIND) and without reservoirs (i.e., NAT) are used to attribute historical changes in surface water storage and extent dynamics over the MRB to natural climate variability and reservoir operation. Further, the probable future impacts of existing dams are assessed using the DamALL simulations, where all existing 86 dams are assumed to be in operation from 1979 (i.e., the beginning of the modeling period).

Results suggest that the interannual flood dynamics in the MRB was dominantly modulated by climate variability over the past four decades. That is, reservoir induced variability is found to be marginal during the historical period, however the impact of reservoirs increased continually over time, becoming readily discernible in recent years (i.e., 2010–2016). Surface water dynamics is found to be altered significantly by reservoirs during the recent period, and results from historical simulations with all dams assumed to have existed from the beginning (i.e., DamALL) suggest that the surface water storage dynamics in the future would be different considerably from that in the past even without additional dams and climate change. Results also indicate that the dynamics of surface water storage and extent depends heavily on reservoir operation strategies, highlighting the need to operate existing and future dams in a way that minimizes the adverse impact on the hydro-ecological systems of the MRB.

There are certain limitations of this study. First, as reservoir bathymetry data are nonexistent for the MRB, bed elevations are parameterized using DEMs, which could introduce some uncertainties in the simulations. Second, this study relies on a generic operation rule because the actual rule curves are not publicly available for any reservoirs in the MRB. And third, tidal effects are not accounted for in our hydrodynamic model, which could have impacted the simulations for the Mekong Delta region. Future studies could improve reservoir bathymetry and operation of individual reservoirs if such data become available. Reservoir bathymetry could also potentially be improved using satellite altimetry and imagery (e.g., Busker et al., 2018; Li et al., 2019), but the application is limited to nonpermanent water areas. For permanent water areas,

hydraulic geometry relationships (e.g., Schaperow et al., 2019) or known reservoir characteristics (e.g., Shin et al., 2019) could be used; however, such methods are generally not suited for deriving high-resolution (e.g., 90 m) reservoir bed elevations.

Despite these limitations, this study provides major advances in simulating integrated river-floodplain--reservoir systems in floodpulse-dominant river systems and isolating the impacts of climate change and reservoir operation on flood dynamics. This study is also the first to simulate the impacts of dams on basin-wide river-floodplain hydrodynamics in the MRB. As there is an unprecedented boom in hydropower dam construction in the MRB and other global river basins (e.g., Amazon and Congo), the impact of reservoirs on global terrestrial hydrology is expected to accelerate in the coming decades. The new modeling framework developed in this study can be used to investigate the potential changes in surface water storage and extent dynamics—which have important hydro-ecological implications—under climate change and the construction of new dams.

Acknowledgments
This study was supported by the National Science Foundation (CAREER Award; Grant#: 1752729) and NASA (Award#: 80NSSC17K0259 and 80NSSC18K1134). Simulations were conducted using Cheyenne (10.5065/D6RX99HX) provided by NCAR's Computational and Information Systems Laboratory, sponsored by the National Science Foundation. Observed river discharge and water level data can be obtained from the Mekong River Commission, and dam database is available from the Research Program on Water, Land, and Ecosystem (https://wle-mekong.cgiar.org/). Global Surface Water data are available from Google Earth Engine, and the Sentinel-1 data can be obtained from Alaska Satellite Facility (https://www.asf.alaska.edu/). Model results used to produce the graphics/tables will be made available upon request through NCAR's Computational and Information Systems Laboratory or HydroShare by the Consortium of Universities for the Advancement of Hydrologic Science Inc. (CUAHSI). The Multi-Error-Removed Improved-Terrain DEM (MERIT DEM) and MERIT DEM-based Hydrography data (MERIT Hydro) are freely available for research and education purposes from the developer's webpage (http://hydro.iis.u-tokyo.ac.jp/~yamadai/MERIT_DEM/ and http://hydro.iis.u-tokyo.ac.jp/~yamadai/MERIT_Hydro/). We thank William McConnell for the comments that helped improve the manuscript.

References

Aggarwal, S. K., Saini, L. M., & Kumar, A. (2009). Electricity price forecasting in deregulated markets: A review and evaluation. *International Journal of Electrical Power & Energy Systems*, *31*(1), 13–22. https://doi.org/10.1016/j.ijepes.2008.09.003

Akter, A., & Babel, M. S. (2012). Hydrological modeling of the Mun River basin in Thailand. *Journal of Hydrology*, *452–453*, 232–246. https://doi.org/10.1016/j.jhydrol.2012.05.059

Angarita, H., Wickel, A. J., Sieber, J., Chavarro, J., Maldonado-Ocampo, J. A., Herrera-R, G. A., et al. (2018). Basin-scale impacts of hydropower development on the Mompós Depression wetlands, Colombia. *Hydrology and Earth System Sciences*, *22*(5), 2839–2865. https://doi.org/10.5194/hess-22-2839-2018

Arias, M. E., Piman, T., Lauri, H., Cochrane, T. A., & Kummu, M. (2014). Dams on Mekong tributaries as significant contributors of hydrological alterations to the Tonle Sap Floodplain in Cambodia. *Hydrology and Earth System Sciences*, *18*(12), 5303–5315. https://doi.org/10.5194/hess-18-5303-2014

Arias, M. E., Cochrane, T. A., & Elliott, V. (2014). Modelling future changes of habitat and fauna in the Tonle Sap wetland of the Mekong. *Environmental Conservation*, *41*(2), 165–175. https://doi.org/10.1017/S0376892913000283

Arias, M. E., Holtgrieve, G. W., Ngor, P. B., Dang, T. D., & Piman, T. (2019). Maintaining perspective of ongoing environmental change in the Mekong floodplains. *Current Opinion in Environmental Sustainability*, *37*(February), 1–7. https://doi.org/10.1016/j.cosust.2019.01.002

Biemans, H., Haddeland, I., Kabat, P., Ludwig, F., Hutjes, R. W. A., Heinke, J., et al. (2011). Impact of reservoirs on river discharge and irrigation water supply during the 20th century. *Water Resources Research*, *47*(3). https://doi.org/10.1029/2009WR008929

Binnie, G. M. (1987). Masonry and concrete dams 1880-1941. *Industrial Archaeology Review*, *10*(1), 41–58. https://doi.org/10.1179/iar.1987.10.1.41

Bonnema, M., & Hossain, F. (2017). Inferring reservoir operating patterns across the Mekong Basin using only space observations. *Water Resources Research*, *53*, 3791–3810. https://doi.org/10.1002/2016WR019978

Bouvet, A., Le Toan, T., & Lam-Dao, N. (2009). Monitoring of the rice cropping system in the Mekong Delta using ENVISAT/ASAR dual polarization data. *IEEE Transactions on Geoscience and Remote Sensing*, *47*(2), 517–526. https://doi.org/10.1109/TGRS.2008.2007963

Bunn, S. E., & Arthington, A. H. (2002). Basic principles and ecological consequences of altered flow regimes for aquatic biodiversity. *Environmental Management*, *30*(4), 492–507. https://doi.org/10.1007/s00267-002-2737-0

Burbano, M., Shin, S., Nguyen, K., & Pokhrel, Y. (2020). Hydrologic changes, dam construction, and the shift in dietary protein in the lower Mekong River Basin. *Journal of Hydrology*, *581*, 124,454. https://doi.org/10.1016/j.jhydrol.2019.124454

Busker, T., de Roo, A., Gelati, E., Schwatke, C., Adamovic, M., Bisselink, B., et al. (2018). A global lake and reservoir volume analysis using a surface water dataset and satellite altimetry. *Hydrology and Earth System Sciences Discussions*, 1–32. https://doi.org/10.5194/hess-2018-21

Chao, B. F., Wu, Y. H., & Li, Y. S. (2008). Impact of artificial reservoir water impoundment on global sea level. *Science*, *320*(5873), 212 LP–214.

Dang, T. D., Chowdhury, A. K., & Galelli, S. (2019). On the representation of water reservoir storage and operations in large-scale hydrological models: Implications on model parameterization and climate change impact assessments. *Hydrology and Earth System Sciences Discussions*, 1–34. https://doi.org/10.5194/hess-2019-334

Dang, T. D., Cochrane, T. A., Arias, M. E., & Tri, V. P. D. (2018). Future hydrological alterations in the Mekong Delta under the impact of water resources development, land subsidence and sea level rise. *Journal of Hydrology: Regional Studies*, *15*, 119–133. https://doi.org/10.1016/j.ejrh.2017.12.002

Delgado, J. M., Merz, B., & Apel, H. (2012). A climate-flood link for the lower Mekong River. *Hydrology and Earth System Sciences*, *16*(5), 1533–1541. https://doi.org/10.5194/hess-16-1533-2012

Duc Tran, D., van Halsema, G., Hellegers, P. J. G. J., Phi Hoang, L., Quang Tran, T., Kummu, M., & Ludwig, F. (2018). Assessing impacts of dike construction on the flood dynamics of the Mekong Delta. *Hydrology and Earth System Sciences*, *22*(3), 1875–1896. https://doi.org/10.5194/hess-22-1875-2018

Dynesius, M., & Nilsson, C. (1994). Fragmentation and flow regulation of river systems in the northern third of the world. *Science*, *266*. https://doi.org/10.1126/science.266.5186.753

El Hajj, M., Baghdadi, N., Bazzi, H., & Zribi, M. (2019). Penetration analysis of SAR signals in the C and L bands for wheat, maize, and grasslands. *Remote Sensing*, *11*(1), 31. https://doi.org/10.3390/rs11010031

Erban, L. E., Gorelick, S. M., & Zebker, H. A. (2014). Groundwater extraction, land subsidence, and sea-level rise in the Mekong Delta, Vietnam. *Environmental Research Letters*, *9*(8), 084010. https://doi.org/10.1088/1748-9326/9/8/084010

Fencl, J. S., Mather, M. E., Costigan, K. H., & Daniels, M. D. (2015). How big of an effect do small dams have? Using geomorphological footprints to quantify spatial impact of low-head dams and identify patterns of across-dam variation. *PLoS ONE*, *10*(11), e0141210. https://doi.org/10.1371/journal.pone.0141210

Fredén, F. (2011). Impacts of dams on lowland agriculture in the Mekong River catchment (PhD Thesis). Lund University.
Gernaat, D. E. H. J., Bogaart, P. W., van Vuuren, D. P., Biemans, H., & Niessink, R. (2017). High-resolution assessment of global technical and economic hydropower potential. *Nature Energy*, *2*(10), 821–828. https://doi.org/10.1038/s41560-017-0006-y
Górski, K., van den Bosch, L. V., van de Wolfshaar, K. E., Middelkoop, H., Nagelkerke, L. A. J., Filippov, O. V., et al. (2012). post-damming flow regime development in a large lowland river (Volga, Russian Federation): Implications for floodplain inundation and fisheries. *River Research and Applications*, *28*(8), 1121–1134. https://doi.org/10.1002/rra.1499
Graf, W. L. (1999). Dam nation: A geographic census of American dams and their large-scale hydrologic impacts. *Water Resources Research*, *35*(4), 1305–1311. https://doi.org/10.1029/1999WR900016
Greathouse, E. A., Pringle, C. M., & Holmquist, J. G. (2006). Conservation and management of migratory fauna: Dams in tropical streams of Puerto Rico. *Aquatic Conservation: Marine and Freshwater Ecosystems*, *16*(7), 695–712. https://doi.org/10.1002/aqc.804
Grill, G., Lehner, B., Thieme, M., Geenen, B., Tickner, D., Antonelli, F., et al. (2019). Mapping the world's free-flowing rivers. *Nature*, *569*(7755), 215–221. https://doi.org/10.1038/s41586-019-1111-9
Grumbine, R. E., & Xu, J. (2011). Mekong hydropower development. *Science*, *332*(6026), 178–179. https://doi.org/10.1126/science.1200990
Gupta, H., Kao, S. J., & Dai, M. (2012). The role of mega dams in reducing sediment fluxes: A case study of large Asian rivers. *Journal of Hydrology*, *464–465*, 447–458. https://doi.org/10.1016/j.jhydrol.2012.07.038
Han, Z., Long, D., Fang, Y., Hou, A., & Hong, Y. (2019). Impacts of climate change and human activities on the flow regime of the dammed Lancang River in Southwest China. *Journal of Hydrology*, *570*, 96–105. https://doi.org/10.1016/j.jhydrol.2018.12.048
Hanasaki, N., Kanae, S., & Oki, T. (2006). A reservoir operation scheme for global river routing models. *Journal of Hydrology*, *327*(1–2), 22–41. https://doi.org/10.1016/j.jhydrol.2005.11.011
Hess, L. L., Melack, J. M., & Simonett, D. S. (1990). Radar detection of flooding beneath the forest canopy: A review. *International Journal of Remote Sensing*, *11*(7), 1313–1325. https://doi.org/10.1080/01431169008955095
Hoes, O. A. C., Meijer, L. J. J., van der Ent, R. J., & van de Giesen, N. C. (2017). Systematic high-resolution assessment of global hydropower potential. *PLoS ONE*, *12*(2), e0171844. https://doi.org/10.1371/journal.pone.0171844
Huang, X., Ziniti, B., Torbick, N., & Ducey, M. (2018). Assessment of forest above ground biomass estimation using multi-temporal C-band Sentinel-1 and Polarimetric L-band PALSAR-2 data. *Remote Sensing*, *10*(9), 1424. https://doi.org/10.3390/rs10091424
Ikeuchi, H., Hirabayashi, Y., Yamazaki, D., Muis, S., Ward, P. J., Winsemius, H. C., et al. (2017). Compound simulation of fluvial floods and storm surges in a global coupled river-coast flood model: Model development and its application to 2007 Cyclone Sidr in Bangladesh. *Journal of Advances in Modeling Earth Systems*, *9*, 1847–1862. https://doi.org/10.1002/2017MS000943
Jardine, T. D., Pusey, B. J., Hamilton, S. K., Pettit, N. E., Davies, P. M., Douglas, M. M., et al. (2012). Fish mediate high food web connectivity in the lower reaches of a tropical floodplain river. *Oecologia*, *168*(3), 829–838. https://doi.org/10.1007/s00442-011-2148-0
Junk, W. J., Bayley, P. B., & Sparks, R. E. (1989). The flood-pulse concept in river-floodplain systems. In D. P. Dodge (Ed.), *Proceedings of the International Large River Symposium (LARS)*, *Canadian Special Publication of Fisheries and Aquatic Sciences*, (Vol. 106, pp. 110–127). Ontario, Canada: Fisheries and Oceans Canada.
Latrubesse, E. M., Arima, E. Y., Dunne, T., Park, E., Baker, V. R., D'Horta, F. M., et al. (2017). Damming the rivers of the Amazon basin. *Nature*, *546*(7658), 363–369. https://doi.org/10.1038/nature22333
Lauri, H., de Moel, H., Ward, P. J., Räsänen, T. A., Keskinen, M., & Kummu, M. (2012). Future changes in Mekong River hydrology: Impact of climate change and reservoir operation on discharge. *Hydrology and Earth System Sciences*, *16*(12), 4603–4619. https://doi.org/10.5194/hess-16-4603-2012
Lehner, B., Liermann, C. R., Revenga, C., Vörösmarty, C., Fekete, B., Crouzet, P., et al. (2011). High-resolution mapping of the world's reservoirs and dams for sustainable river-flow management. *Frontiers in Ecology and the Environment*, *9*(9), 494–502. https://doi.org/10.1890/100125
Li, Y., Gao, H., Jasinski, M. F., Zhang, S., & Stoll, J. D. (2019). Deriving high-resolution reservoir bathymetry from ICESat-2 prototype photon-counting Lidar and Landsat imagery. *IEEE Transactions on Geoscience and Remote Sensing*, 1–11. https://doi.org/10.1109/TGRS.2019.2917012
Lin, Z., & Qi, J. (2017). Hydro-dam—A nature-based solution or an ecological problem: The fate of the Tonlé Sap Lake. *Environmental Research*, *158*, 24–32. https://doi.org/10.1016/j.envres.2017.05.016
Mateo, C. M., Hanasaki, N., Komori, D., Tanaka, K., Kiguchi, M., Champathong, A., et al. (2014). Assessing the impacts of reservoir operation to floodplain inundation by combining hydrological, reservoir management, and hydrodynamic models. *Water Resources Research*, *50*, 7245–7266. https://doi.org/10.1002/2013WR014845
MRC. (2005). *Overview of the hydrology of the Mekong Basin*. Vientiane: Lao PDR.
Minh, H. V. T., Kurasaki, M., Ty, T. V., Tran, D. Q., Le, K. N., Avtar, R., et al. (2019). Effects of multi-dike protection systems on surface water quality in the Vietnamese Mekong Delta. *Water*, *11*(5), 1010. https://doi.org/10.3390/w11051010
Nelson, A., Setiyono, T., Rala, A., Quicho, E., Raviz, J., Abonete, P., et al. (2014). Towards an operational SAR-based rice monitoring system in Asia: Examples from 13 demonstration sites across Asia in the RIICE project. *Remote Sensing*, *6*(11), 10773–10812. https://doi.org/10.3390/rs61110773
Nilsson, C., Reidy, C. A., Dynesius, M., & Revenga, C. (2005). Fragmentation and flow regulation of the world's large river systems. *Science*, *308*. https://doi.org/10.1126/science.1107887
Null, S. E., Medellín-Azuara, J., Escriva-Bou, A., Lent, M., & Lund, J. R. (2014). Optimizing the dammed: Water supply losses and fish habitat gains from dam removal in California. *Journal of Environmental Management*, *136*, 121–131. https://doi.org/10.1016/j.jenvman.2014.01.024
Oeurng, C., Cochrane, T., Chung, S., Kondolf, M., Piman, T., & Arias, M. (2019). Assessing climate change impacts on river flows in the Tonle Sap Lake Basin, Cambodia. *Water*, *11*(3), 618. https://doi.org/10.3390/w11030618
Oki, T., & Kanae, S. (2006). Global hydrological cycles and world water resources. *Science*, *313*(5790), 1068–1072. https://doi.org/10.1126/science.1128845
Pekel, J.-F., Cottam, A., Gorelick, N., & Belward, A. S. (2016). High-resolution mapping of global surface water and its long-term changes. *Nature*, *540*(7633), 418–422. https://doi.org/10.1038/nature20584
Piman, T., Lennaerts, T., & Southalack, P. (2013). Assessment of hydrological changes in the lower Mekong Basin from basin-wide development scenarios. *Hydrological Processes*, *27*(15), 2115–2125. https://doi.org/10.1002/hyp.9764
Poff, N. L. R., & Schmidt, J. C. (2016). How dams can go with the flow. *Science*, *353*(6304), 1099–1100. https://doi.org/10.1126/science.aah4926
Pohl, M. M. (2002). Bringing down our dams: Trends in American dam removal rationales. *Journal of the American Water Resources Association*, *38*(6), 1511–1519. https://doi.org/10.1111/j.1752-1688.2002.tb04361.x

Pokhrel, Y., Burbano, M., Roush, J., Kang, H., Sridhar, V., & Hyndman, D. (2018). A review of the integrated effects of changing climate, land use, and dams on Mekong River hydrology. *Water*, *10*(3), 266. https://doi.org/10.3390/w10030266

Pokhrel, Y., Hanasaki, N., Koirala, S., Cho, J., Yeh, P. J.-F., Kim, H., et al. (2012). Incorporating anthropogenic water regulation modules into a land surface model. *Journal of Hydrometeorology*, *13*(1), 255–269. https://doi.org/10.1175/JHM-D-11-013.1

Pokhrel, Y., Shin, S., Lin, Z., Yamazaki, D., & Qi, J. (2018). Potential disruption of flood dynamics in the lower Mekong River Basin due to upstream flow regulation. *Scientific Reports*, *8*(1), 17767. https://doi.org/10.1038/s41598-018-35823-4

Pokhrel, Y. N., Hanasaki, N., Yeh, P. J.-F., Yamada, T. J., Kanae, S., & Oki, T. (2012). Model estimates of sea-level change due to anthropogenic impacts on terrestrial water storage. *Nature Geoscience*, *5*(6), 389–392. https://doi.org/10.1038/ngeo1476

Pokhrel, Y. N., Koirala, S., Yeh, P. J.-F., Hanasaki, N., Longuevergne, L., Kanae, S., & Oki, T. (2015). Incorporation of groundwater pumping in a global land surface model with the representation of human impacts. *Water Resources Research*, *51*, 78–96. https://doi.org/10.1002/2014WR015602

Räsänen, T. A., Koponen, J., Lauri, H., & Kummu, M. (2012). Downstream hydrological impacts of hydropower development in the upper Mekong Basin. *Water Resources Management*, *26*(12), 3495–3513. https://doi.org/10.1007/s11269-012-0087-0

Räsänen, T. A., Someth, P., Lauri, H., Koponen, J., Sarkkula, J., & Kummu, M. (2017). Observed river discharge changes due to hydropower operations in the upper Mekong Basin. *Journal of Hydrology*, *545*, 28–41. https://doi.org/10.1016/j.jhydrol.2016.12.023

Renwick, W. H., Smith, S. V., Bartley, J. D., & Buddemeier, R. W. (2005). The role of impoundments in the sediment budget of the conterminous United States. *Geomorphology*, *71*(1–2), 99–111. https://doi.org/10.1016/j.geomorph.2004.01.010

Sabo, J. L., Ruhi, A., Holtgrieve, G. W., Elliott, V., Arias, M. E., Ngor, P. B., et al. (2017). Designing river flows to improve food security futures in the lower Mekong Basin. *Science*, *358*(6368), eaao1053. https://doi.org/10.1126/science.aao1053

Schaperow, J. R., Li, D., Margulis, S. A., & Lettenmaier, D. P. (2019). A curve-fitting method for estimating bathymetry from water surface height and width. *Water Resources Research*, *55*, 4288–4303. https://doi.org/10.1029/2019WR024938

Shin, S., Pokhrel, Y., & Miguez-Macho, G. (2019). High-resolution modeling of reservoir release and storage dynamics at the continental scale. *Water Resources Research*, *55*, 787–810. https://doi.org/10.1029/2018WR023025

Smajgl, A., Toan, T. Q., Nhan, D. K., Ward, J., Trung, N. H., Tri, L. Q., et al. (2015). Responding to rising sea levels in the Mekong Delta. *Nature Climate Change*, *5*(2), 167–174. https://doi.org/10.1038/nclimate2469

Sridhar, V., Kang, H., & Ali, S. A. (2019). Human-induced alterations to land use and climate and their responses for hydrology and water management in the Mekong River Basin. *Water*, *11*(6), 1307. https://doi.org/10.3390/w11061307

Stone, R. (2016). Dam-building threatens Mekong fisheries. *Science*, *354*(6316), 1084–1085. https://doi.org/10.1126/science.354.6316.1084

Takata, K., Emori, S., & Watanabe, T. (2003). Development of the minimal advanced treatments of surface interaction and runoff. *Global and Planetary Change*, *38*(1–2), 209–222. https://doi.org/10.1016/S0921-8181(03)00030-4

Tan, Y., Bryan, B., & Hugo, G. (2005). Development, land-use change and rural resettlement capacity: A case study of the Three Gorges Project, China. *Australian Geographer*, *36*(2), 201–220. https://doi.org/10.1080/00049180500153484

Timpe, K., & Kaplan, D. (2017). The changing hydrology of a dammed Amazon. *Science Advances*, *3*(11) Retrieved from. http://advances.sciencemag.org/content/3/11/e1700611.abstract

Torbick, N., Chowdhury, D., Salas, W., & Qi, J. (2017). Monitoring rice agriculture across Myanmar using time series Sentinel-1 assisted by Landsat-8 and PALSAR-2. *Remote Sensing*, *9*(2), 119. https://doi.org/10.3390/rs9020119

Torbick, N., Huang, X., Ziniti, B., Johnson, D., Masek, J., & Reba, M. (2018). Fusion of moderate resolution Earth observations for operational crop type mapping. *Remote Sensing*, *10*(7), 1058. https://doi.org/10.3390/rs10071058

Torbick, N., Salas, W., Chowdhury, D., Ingraham, P., & Trinh, M. (2017). Mapping rice greenhouse gas emissions in the Red River Delta, Vietnam. *Carbon Management*, *8*(1), 99–108. https://doi.org/10.1080/17583004.2016.1275816

Trung, L. D., Duc, N. A., Nguyen, L. T., Thai, T. H., Khan, A., Rautenstrauch, K., & Schmidt, C. (2018). Assessing cumulative impacts of the proposed lower Mekong Basin hydropower cascade on the Mekong River floodplains and Delta—Overview of integrated modeling methods and results. *Journal of Hydrology*. https://doi.org/10.1016/j.jhydrol.2018.01.029

Urbazaev, M., Cremer, F., Migliavacca, M., Reichstein, M., Schmullius, C., & Thiel, C. (2018). Potential of multi-temporal ALOS-2 PALSAR-2 ScanSAR data for vegetation height estimation in tropical forests of Mexico. *Remote Sensing*, *10*(8), 1277. https://doi.org/10.3390/rs10081277

van Bemmelen, C. W. T., Mann, M., de Ridder, M. P., Rutten, M. M., & van de Giesen, N. C. (2016). Determining water reservoir characteristics with global elevation data. *Geophysical Research Letters*, *43*, 11278–11286. https://doi.org/10.1002/2016GL069816

Vörösmarty, C. J., McIntyre, P. B., Gessner, M. O., Dudgeon, D., Prusevich, A., Green, P., et al. (2010). Global threats to human water security and river biodiversity. *Nature*, *467*(7315), 555–561. https://doi.org/10.1038/nature09440

Wang, P., Dong, S., & Lassoie, J. P. (2014). Large dams in China: An overview of history, distribution, and case studies. In *The Large Dam Dilemma*, (pp. 25–41). Dordrecht: Springer Netherlands. https://doi.org/10.1007/978-94-007-7630-2_2

Wang, W., Lu, H., Ruby Leung, L., Li, H.-Y., Zhao, J., Tian, F., et al. (2017). Dam construction in Lancang-Mekong River Basin could mitigate future flood risk from warming-induced intensified rainfall. *Geophysical Research Letters*, *44*, 10378–10386. https://doi.org/10.1002/2017GL075037

Wang, W., Lu, H., Yang, D., Sothea, K., Jiao, Y., Gao, B., et al. (2016). Modelling hydrologic processes in the Mekong River Basin using a distributed model driven by satellite precipitation and rain gauge observations. *PLoS ONE*, *11*(3), e0152229. https://doi.org/10.1371/journal.pone.0152229

Warfe, D. M., Jardine, T. D., Pettit, N. E., Hamilton, S. K., Pusey, B. J., Bunn, S. E., et al. (2013). Productivity, disturbance and ecosystem size have no influence on food chain length in seasonally connected rivers. *PLoS ONE*, *8*(6), e66240. https://doi.org/10.1371/journal.pone.0066240

Weedon, G. P., Balsamo, G., Bellouin, N., Gomes, S., Best, M. J., & Viterbo, P. (2018). *The WFDEI Meteorological Forcing Data*. Boulder, CO: Research Data Archive at the National Center for Atmospheric Research, Computational and Information Systems Laboratory. Retrieved from. http://rda.ucar.edu/datasets/ds314.2/

Wei, G., Yang, Z., Cui, B., Li, B., Chen, H., Bai, J., & Dong, S. (2009). Impact of dam construction on water quality and water self-purification capacity of the Lancang River, China. *Water Resources Management*, *23*(9), 1763–1780. https://doi.org/10.1007/s11269-008-9351-8

Weron, R. (2014). Electricity price forecasting: A review of the state-of-the-art with a look into the future. *International Journal of Forecasting*, *30*(4), 1030–1081. https://doi.org/10.1016/j.ijforecast.2014.08.008

Wild, T. B., & Loucks, D. P. (2014). Managing flow, sediment, and hydropower regimes in the Sre Pok, Se San, and Se Kong Rivers of the Mekong basin. *Water Resources Research*, *50*, 5141–5157. https://doi.org/10.1002/2014WR015457

Winemiller, K. O., McIntyre, P. B., Castello, L., Fluet-Chouinard, E., Giarrizzo, T., Nam, S., et al. (2016). Balancing hydropower and biodiversity in the Amazon, Congo, and Mekong. *Science*, *351*(6269), 128–129. https://doi.org/10.1126/science.aac7082

World Commission on Dams (2000). *Dams and development: A new framework for decision-making*, (1st ed.). Sterling, VA: Taylor & Francis.

Yamazaki, D., Ikeshima, D., Sosa, J., Bates, P. D., Allen, G., & Pavelsky, T. (2019). MERIT Hydro: A high-resolution global hydrography map based on latest topography datasets. *Water Resources Research*, *55*, 5053–5073. https://doi.org/10.1029/2019WR024873

Yamazaki, D., de Almeida, G. A. M., & Bates, P. D. (2013). Improving computational efficiency in global river models by implementing the local inertial flow equation and a vector-based river network map. *Water Resources Research*, *49*, 7221–7235. https://doi.org/10.1002/wrcr.20552

Yamazaki, D., Ikeshima, D., Tawatari, R., Yamaguchi, T., O'Loughlin, F., Neal, J. C., et al. (2017). A high-accuracy map of global terrain elevations. *Geophysical Research Letters*, *44*, 5844–5853. https://doi.org/10.1002/2017GL072874

Yamazaki, D., Kanae, S., Kim, H., & Oki, T. (2011). A physically based description of floodplain inundation dynamics in a global river routing model. *Water Resources Research*, *47*, W04501. https://doi.org/10.1029/2010WR009726

Yamazaki, D., Lee, H., Alsdorf, D. E., Dutra, E., Kim, H., Kanae, S., & Oki, T. (2012). Analysis of the water level dynamics simulated by a global river model: A case study in the Amazon River. *Water Resources Research*, *48*, W09508. https://doi.org/10.1029/2012WR011869

Yamazaki, D., Sato, T., Kanae, S., Hirabayashi, Y., & Bates, P. D. (2014). Regional flood dynamics in a bifurcating mega delta simulated in a global river model. *Geophysical Research Letters*, *41*, 3127–3135. https://doi.org/10.1002/2014GL059744

Zarfl, C., Lumsdon, A. E., Berlekamp, J., Tydecks, L., & Tockner, K. (2015). A global boom in hydropower dam construction. *Aquatic Sciences*, *77*(1), 161–170. https://doi.org/10.1007/s00027-014-0377-0

Zhou, Y., Hejazi, M., Smith, S., Edmonds, J., Li, H., Clarke, L., et al. (2015). A comprehensive view of global potential for hydro-generated electricity. *Energy & Environmental Science*, *8*(9), 2622–2633. https://doi.org/10.1039/C5EE00888C

Ziv, G., Baran, E., Nam, S., Rodriguez-Iturbe, I., & Levin, S. A. (2012). Trading-off fish biodiversity, food security, and hydropower in the Mekong River Basin. *Proceedings of the National Academy of Sciences*, *109*(15), 5609–5614. https://doi.org/10.1073/pnas.1201423109